VACUUM ULTRAVIOLET SPECTROSCOPY OF DIELECTRIC SURFACE FLASHOVER IN ATMOSPHERE

by

GEORGE RUSSELL LAITY, B.S.

A THESIS

IN

ELECTRICAL ENGINEERING

Submitted to the Graduate Faculty
of Texas Tech University in
Partial Fulfillment of
the Requirements for
the Degree of

MASTER OF SCIENCE

IN

ELECTRICAL ENGINEERING

Approved

Andreas A. Neuber
Chairperson of the Committee

Hermann G. Krompholz

Fred Hartmeister
Dean of the Graduate School

May, 2010

ACKNOWLEDGEMENTS

In general I would like to thank the P3E faculty for their support during my time in the laboratory. I would first like to thank Dr. Neuber for not only serving as chairman of my committee, but also for understanding my background and by pushing me into being a better scientist during my transition into engineering. I would especially like to thank Dr. Frank for the many conversations during his time at Texas Tech, and for his insight on my project. I would also like to thank Dr. Krompholz and Dr. Hatfield for their interest in my work, and for adding their expertise into the mix of knowledge I've used during my time on this research.

Next I would like to thank all of my colleagues in the Center for Pulsed Power and Power Electronics at Texas Tech. Special thanks to Garrett for his role as my partner on this work, and for all the time spent with me investigating new ideas both successful and not during the last two years. I would like to thank Dr. Krile for his time explaining to me the ICCD systems, and for passing the unwritten knowledge of these systems to me during our "troubleshooting" sessions. I would also like to thank my fellow graduate students in the laboratory for all the conversations and brainstorming sessions concerning both my work and others.

Finally I would like to thank my father, who for the past 24 years has helped me in scouting, maintained my faith, and promoted my interest in engineering and science throughout my life.

CONTENTS

ABSTRACT

Vacuum ultraviolet (VUV) emission is believed to play a major role in the development of plasma streamers in pulsed atmospheric discharges, but studies of VUV radiation are difficult to make for pulsed experiments at atmospheric pressures. Since VUV light is absorbed in most materials and gases, consideration must be given to the construction of the experimental apparatus and selection of optics used in spectral instruments for VUV analysis. Of highest interest is the VUV emission during the initial stage of pulsed atmospheric discharges, which has a typical duration in the nanosecond regime.

An experiment was designed to study this fast initial stage of VUV emission coupled with fast optical imaging of streamer propagation, both with temporal resolution on the order of nanoseconds. VUV emission with sufficient intensity to be detected on the nanosecond timescale was observed from unipolar surface flashover events excited from a repetitive solid-state high voltage pulser. VUV emission is captured utilizing both photomultiplier and ICCD detectors during the fast stage of streamer propagation. It was concluded that most VUV emission occurs during the initial stage leading into voltage collapse, with limited VUV activity during the remaining discharge. Spectral analysis was performed through the use of simulation software, and virtually all emission was attributed to excited oxygen and nitrogen. Lastly, an electrostatic model was created with results consistent with the observed streamer characteristics for a number of electric field geometries.

**This work was supported by the U.S. Air Force Office of Scientific Research*

LIST OF TABLES

LIST OF FIGURES

CHAPTER 1

INTRODUCTION

The fundamental physical relationships which define electrical breakdown phenomena are widely described in literature [1-3], but the understanding of the transition from streamer into spark discharge is still highly qualitative. The accepted theory argues that photons, which are emitted from excited molecules resulting from electron collisions, travel ahead of small electron avalanches and ionize molecules which form new avalanches. This phenomenon is known as *streamer propagation*, and is widely believed to play a leading role in the initial development of discharges at atmospheric pressure in the high field regime [4-5]. The velocity of these propagating streamers during this first stage is a significant factor which can characterize breakdown behavior, but requires a spatial resolution on the order of microns to measure accurately for a spark gap length on the order of millimeters.

More importantly the role of vacuum ultraviolet light (VUV) is also of central interest for breakdown studies involving streamers. If it is assumed that streamer propagation is primarily fueled from photoionization processes [6-7], from basic principles it must be concluded that only VUV light is energetic enough to ionize common atmospheric gases such as oxygen and nitrogen. While emission from continuous VUV sources has been investigated [8], it is desirable to quantitatively investigate the role of VUV emission for pulsed atmospheric discharges of interest in the aerospace community (for example on the interface between atmosphere and vacuum for some high power systems). Because

most VUV is absorbed in short distances in air [9], it is required that emission from the discharge be transitioned into vacuum to enable VUV propagation through an optical instrument for spectral analysis. VUV light is strongly absorbed in most materials as well [10], and so the transition window which separates atmosphere from vacuum, the spectral apparatus, and detection mechanisms must be transmissive to VUV radiation.

The following chapters discuss the relevant physics for streamer formation in atmosphere, followed by an overview of emission physics of importance in spectral measurement and simulation. Discussion of VUV absorption is given along with the relevant results of previous UV studies of interest which form a background for this work at TTU. Following these sections is a detailed discussion of the experiment designed to study VUV emission and streamer propagation of pulsed atmospheric discharges, including information on both the electrical and optical diagnostic systems. Finally, the experimental results are broken down in the final chapter into sections concerning VUV absorption and emission measurements, electrical breakdown waveforms, streamer imaging, and corresponding spectral and electrostatic simulation outcomes. The results of this study are briefly summarized at the end of the document, along with suggested future work.

CHAPTER 2

BACKGROUND THEORY

Before discussion can begin on this experimental study of fast electrical breakdown, one must be versed with the underlying physics that dominate streamer type discharges. The following section contains a brief explanation of the physics of ionization processes and streamer theory, along with the fundamental concepts of spectral physics and measurement techniques which are relevant in this study. Detailed discussion of these topics is widely available in literature [1-3, 11] and is only touched upon here.

2.1 Ionization Processes

Assuming the availability of "free" or primary electrons, a number of processes can take place which produce secondary electrons which fuel the breakdown process. The mechanism by which electrons are freed from atoms or molecules is referred to as ionization, and frequently the underlying conditions require that the electron be given energy large enough to escape its local potential energy. In this process a positively charged ion and negatively charged secondary electron are produced. While a number of mechanisms exist which can directly excite or ionize molecules, the only processes which are of interest in this study are ionization by collision and by photon capture (or photoionization). Because the central concept of this work is the production of vacuum ultraviolet photons and their subsequent effect on breakdown, the emphasis is given to

photon and electron production in high field regions, where photon emission and absorption are most likely to occur.

2.1.1 Ionization by Collision

Electron production from collision is widely considered to be a significant process which contributes to volume charge production in gas discharges [1]. When electrons are accelerated in the high field regions of electrodes under a static potential difference, the electrons can gain significant energy and collide with gas molecules. If the amount of energy transfer from the accelerated electron is large enough, the molecule can become excited or ionized. Processes which convert kinetic energy into energy used for ionization are referred in literature as first order processes [12]:

$$AB + e \rightarrow AB^{+} + 2e \qquad \textit{(Direct Ionization)} \tag{2.1}$$

$$AB + e \rightarrow A^{+} + B + 2e \qquad \textit{(Dissociative Ionization)} \tag{2.2}$$

A common example of a second order process frequently found in gas discharges is the Penning effect, where an excited molecule collides with a ground molecule and the transfer of excess energy is large enough to ionize the ground molecule [2]:

$$A^{*} + B \rightarrow A + B^{+} + e \qquad \textit{(Penning Effect)} \tag{2.3}$$

In general, ionization by electron collision has been studied significantly and can be summarized not necessarily by the number of ionizations per time interval (ionization *frequency*) but more frequently by the ionizations caused by electron avalanche between

anode and cathode (ionization per unit distance in the direction of the applied field) [1]. The ionization rate from avalanche due to this field is known in literature as the 1st Townsend ionization coefficient (α):

$$\alpha = Ape^{-Bp/E} \tag{2.4}$$

For atmospheric discharges, this coefficient can be approximated as a function of both applied field (*E*) and pressure (*p*). The coefficients A and B were determined empirically from discharge experiments, and a selection of relevant values for atmospheric gases has been tabulated below from literature [1] (only for the validity range stated):

Table 2.1: Selected ionization coefficients with usable E/p range for some atmospheric gases of interest [1]

Gas	A [$cm^{-1}torr^{-1}$]	B [$V / cm^{-1}torr^{-1}$]	E/p Range
He	3	34	20 - 150
Ar	12	180	100 - 600
N_2	12	342	100 - 600
N_2	8.8	275	27 - 200
Air	15	365	100 - 800
CO_2	20	466	500 - 1000
H_2O	13	290	150 - 1000

2.1.2 Photoionization

While less likely to be a significant process for bulk discharges, the initial nanosecond scale phase of atmospheric discharges can be dominated by photon driven ionization, or photoionization. For a photon to ionize a molecule and free an electron, the photon must have an energy large enough to overcome the molecule's ionization potential (E) [13]:

$$\frac{hc}{\lambda} \geq E \tag{2.5}$$

where the photon's energy is determined by its wavelength (λ), along with Plank's constant (h) and the speed of light in vacuum (c). In general photons do not have enough energy to meet this condition in gas discharges [1], but photons during the initial fast phase of the discharge can gain enough energy if emitted by collisional electrons which have been accelerated in the high field region around the electrodes.

For example, atomic nitrogen and oxygen have ionization energies on the order of 14 eV, and excitation energies on the order of 10 eV [14]. Photons with energies in this range correspond to light in the vacuum ultraviolet (VUV) regime, with wavelengths from 70 to 130 nm. However, it was shown in literature that radiation corresponding to 125 nm can ionize most atmospheric gases [1]. The qualitative explanation is that photons in this range must be able to first excite gas molecules, and then later the molecule re-absorbs a similar photon which ionizes the molecule from an excited state. This process is known as step ionization, and is possible in molecules which exhibit

metastable states. If this step photoionization process plays a role in the initial stage of atmospheric discharges, it is probable that significant emission activity can be observed which correspond to the excitation modes between 120 and 150 nm during this initial stage.

It could also be likely that direct ionization or dissociation of oxygen molecules could result from photons which were radiated by nitrogen molecules, or vice versa (which would be evident from excitation states in the VUV range with wavelengths shorter than 100 nm). Because of the absence of strong cosmic radiation at ground altitude in the laboratory, these UV photons must be emitted from radiating molecules which have been excited during electron collisions in the high field regions. These photons will play a significant role in streamer formation, as discussed in the next section.

2.2 Streamer Formation

Streamers are weakly ionized thin channels which appear in the wake of smaller electron avalanches formed in sufficient electric fields between electrodes [1]. These streamers can eventually combine to alter the local fields in the gap with energy buildup, which can later transition into full spark breakdown. The fundamental concepts of streamer physics and the role of photons in these streamers are of great importance to nanosecond scale breakdown development.

2.2.1 Space Charge Theory

During an electron avalanche, a significant volume of charge is generated due to amplification, which grows exponentially through the gap. As molecules are ionized and charge is generated, secondary electrons and ions begin to collect in the gap. Due to the small mass of the electrons and relative amplitude of applied electric field, the electrons are quickly conducted out of the gap and into the anode. During this time the electrons and ions begin to separate and form a pseudo dipole electric field in the gap (see Figure 2.1a). However the ions, which are on the order of 2000 times more massive than electrons, take longer to conduct away into the cathode, and so a net positive charge begins to fill the ionized space between the electrodes (a concept known in literature as *ambipolar diffusion*) [2]. This positive space charge can draw newly freed electrons towards it instead of the anode which appears far away, and this distortion of the applied field can cause streamers to appear from the gap space instead of the areas of high

applied field around the electrodes. This is essential in the evolution of self contained streamers, and only occurs when the space charge field becomes on the order of the applied field [1].

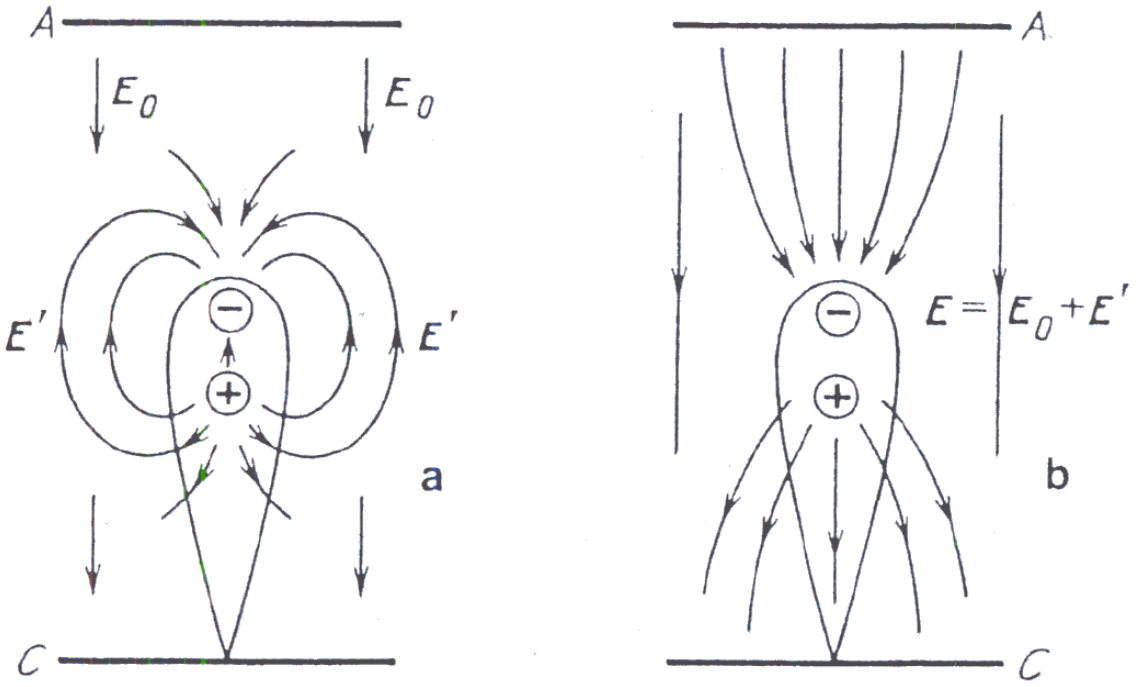

Figure 2.1: (a) Evolution of space charge fields during an electron avalanche, and (b) total resulting field combined from applied and space charge generated fields [1].

2.2.2 Cathode Directed Streamers

If gap distances are on the order of 1 cm and the overvoltage is not too high, sufficient conduction can occur when the local amplification of an electron avalanche cannot gain sufficient size before the electrons reach the anode [1]. The result is that the electrons can ignite processes which propagate back into the gap towards the cathode, a

process known as *cathode directed streamer formation*. The mechanism for the generation of cathode directed streamers is shown in Figure 2.2:

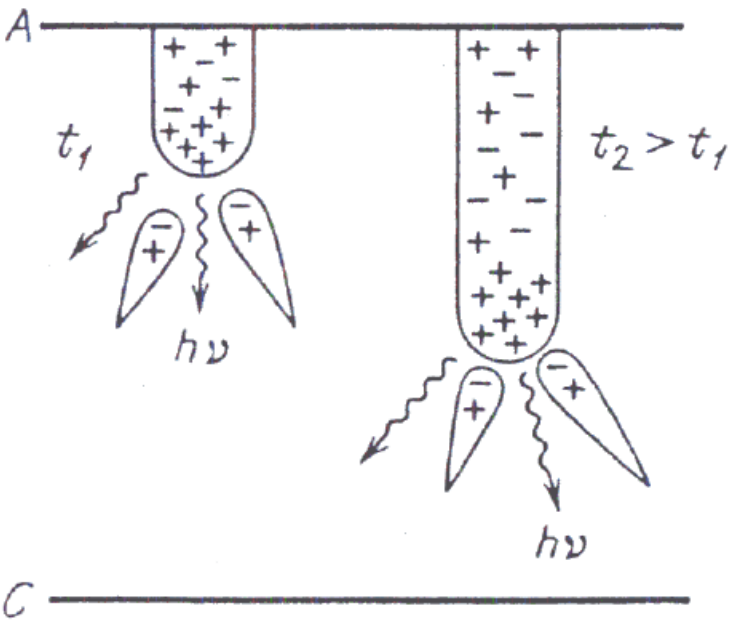

Figure 2.2: Generation and propagation of a cathode directed streamer, shown during two time intervals [1].

The electrons which have accelerated in the high field region near the anode undergo collisions and emit VUV photons into the gap. These photons, through possible step processes discussed in the previous section, ionize molecules located in the gap. The newly freed electrons are quickly accelerated towards the anode, while the more massive positive ion space charge remains and slowly accelerates towards the cathode. More VUV photons are generated from collisional excitation and radiative de-excitation and the process repeats. Most electrons in this process are quickly conducted away into the anode, although they are the driving means for VUV photon production. Eventually the

positive space charge becomes large enough so that smaller electron avalanches are accelerated into the regions of largest ion charge. During this process the most luminous regions are where the most VUV photon production occurs, which happens in the vicinity of the smaller electron avalanches and appear as streamer heads in imaging. When the streamers finally grow to the point where the primary (or leading) streamer connects with the cathode, a long body extends which bridges the electrode gap as a virtual "needle." Sufficient production of streamers will lead to spark breakdown if the electron avalanches meet the so called Meek criterion [1]:

$$\alpha d \approx 20 \tag{2.6}$$

where α is the ionization coefficient, E is the applied electric field, and d is the electrode gap distance. Even still, the primary means for streamer growth is photoionization, and the goal of this research is to determine the impact of VUV photons on these processes as they contribute to high power surface flashover.

2.2.3 Anode Directed Streamers

It is possible under significant overvoltage conditions that the Meek criterion is satisfied for a certain distance d, which is smaller than the gap distance between electrodes [1]. If this is the case, the smaller electron avalanches can transform into streamers before reaching the anode in the first phase, and the streamers will propagate towards both electrodes, appearing from an initial point inside the gap. This event is

known in literature as an *anode directed streamer*, although the process is similar in nature to the cathode directed case (see Figure 2.3). The main body of the leading streamer is now full of electrons accelerating towards the anode, which through collisions emit VUV photons. These photons generate electron / ion pairs which form smaller avalanches, now accelerating away from the main streamer body. Because the other end of the streamer body is still accelerating towards the cathode, electron / ion pairs are generated in the bottom area as well. Eventually ions generated near the anode accelerate towards the cathode, and the electrons generated near the cathode accelerate towards the anode. The resulting mix of electrons and ions in the streamer body forms a quasi-neutral plasma during the time scales relevant for streamer propagation.

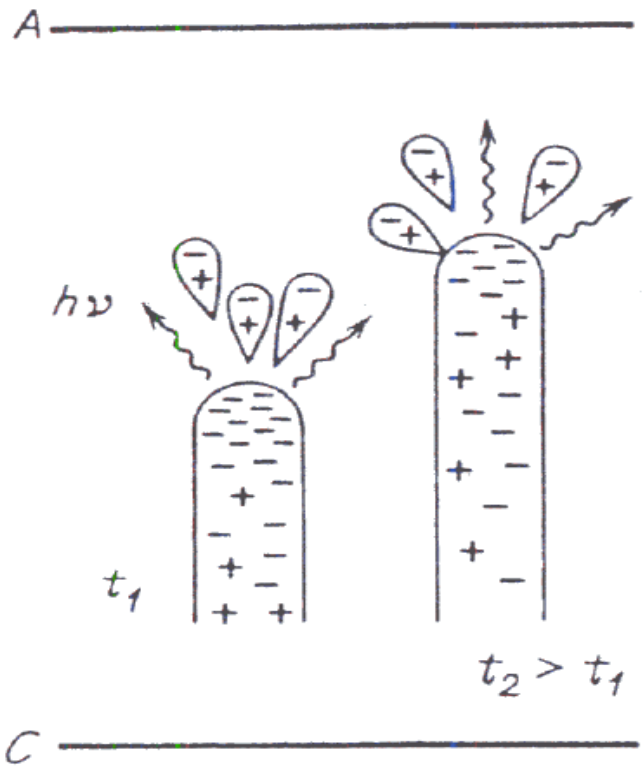

Figure 2.3: Generation and propagation of an anode directed streamer, shown during two time intervals [1].

2.3 Emission Physics

Emission diagnostics can be an extremely useful non-invasive way of gauging the inner properties of a developing plasma, and are used extensively in gas discharge studies. Because this study uses spectroscopy as the primary diagnostic, it is necessary to understand the background theory related to emission physics and the various effects which are observed in spectral line radiation.

2.3.1 Boltzmann Population Density

When an electron makes a transition from one discrete atomic energy level to another, a photon is either emitted or absorbed in the process. The rate by which an electron is able to "jump" from a lower energy level into a higher one is determined solely by its ability to "capture" energy from the environment, in some form. For collision dominated environments in thermodynamic equilibrium, it can be shown from statistical mechanics [11] that a Boltzmann distribution at temperature T accurately determines the population densities of two energy states:

$$\frac{n_2}{n_1} = \frac{g_2}{g_1} e^{-(E_2 - E_1)/kT} \tag{2.7}$$

where n_2 and n_1 are the population densities, g_2 and g_1 are the degeneracies of the energy levels, $E_2 - E_1$ is the energy difference of the two levels, and k is Boltzmann's constant. While the translational temperature ($T_{trans} \approx 300$ K) of the gas molecules remains

relatively unchanged during the discharge timescales, the Boltzmann distribution is acceptable for these studies under the assumption that the plasma develops with an electronic temperature quickly coming to *local thermodynamic equilibrium* (LTE) [11].

The degeneracy and energy levels for a given transition can be tabulated from experiment and calculation, and can later be used in simulation for a given test temperature T to find the ratio of electronic population densities. For this study, this information was taken from the National Institute of Standards and Technology (NIST) Atomic Spectral Database, which is available online [15]. Once these values are known, the exact population density of a specific state can be calculated from the sum of all possible states (known as the *partition function*) and the total gas number (n_0):

$$n_1 = \frac{n_0 \, g_1 \, e^{-E_1 / kT}}{\sum_i g_i \, e^{-E_i / kT}} \tag{2.8}$$

Once the population densities are known, the probability of a decay coupled with photon emission can be calculated from the coefficients of spontaneous emission.

2.3.2 Spontaneous Emission

There are a number of possible transitions (in the form of electromagnetic radiation, e.g. photons) which can take place when an electron exists between one of two energy states. If the electron wave function is at the lower of the two energy levels and interacts with a photon of energy equal to the difference between the two energy levels, the photon

is captured and the electron wave function transitions into the higher energy state in a process known as *absorption*. However, an electron wave function can decay from the top energy level into the lower one, and the energy lost in the process takes the form of an emitted photon in a process known as *spontaneous emission.* One cannot definitely predict the outcome to whether an electron wave function will decay and emit a photon, but instead on average estimate that a number of states with a given population density will undergo a statistical number of decays with a given time constant. Einstein was the first one to estimate this decay from thermodynamic principles, and the rate at which a population of excited states will decay is given by the Einstein coefficient for spontaneous emission, A_{nm}. The units for A_{nm} are s^{-1}, so the product of A_{nm} and the population density n_2 determined from the previous section gives the number of emissions per second. These coefficients have been determined by a combination of theory and experiment, and are available in literature for a variety of transitions of interest [15].

The number of observed emissions can be smaller than the expected theoretical emission number, which can occur in nature from a variety of natural processes collectively known as *quenching*. For example, an excited molecule can interact with another molecule where the transfer of excess energy is enough to ionize or excite the secondary molecule. In this case (*radiationless transfer)* the observed population density for a given excited state could be lower than the theoretical value, because many of the states could be shifting energy by collision and not through radiation. Another possible case is that an emitted photon could be captured (absorbed) by a similar molecule, since

the energy difference is exactly the same in both molecules and thus an electron could move into an excited state. This process is called *re-absorption* or *self absorption* in gases, and is especially likely in cases involving a transition to the ground energy state.

2.3.3 Line Width Estimation

Based on the constructed theory, a gas in local thermodynamic equilibrium with population densities n_2 and n_1 calculated from a Boltzmann distribution at temperature T will spontaneously emit photons of a given wavelength at a rate determined by their Einstein coefficients. The result would be an observed emission line of zero line width, measured exactly at the wavelength given from the energy difference between electronic levels. However, in measurement lines are broadened by a number of mechanisms both natural and instrumental.

The accepted theory from quantum mechanics tells us that it is impossible to know both energy and time content for a given state at the atomic level, a postulate known as the Heisenberg uncertainty principle [16]. As a result, the energy difference for a given transition cannot be exactly calculated as compared to the finite time scales of the Einstein coefficients for spontaneous emission. Because the "error" in the energy states can drift higher or lower statistically, the wavelength of line emitted from a decay of such states will be broadened. It can be shown the profile of this type of line width, known in literature as *natural* line width, can be determined by a Lorentzian distribution [11]:

$$f_L = \frac{1}{\pi}\left[\frac{\gamma}{(x-x_0)^2+\gamma^2}\right] \tag{2.9}$$

where x_0 is the position (wavelength) of the line and γ is a parameter which determines line width. However for most lines in the VUV range, natural broadening is on the order of 10^{-15} m, so it is seldom directly measured.

Also of interest is a mechanism known as *pressure broadening*, which is primarily attributed to the interaction of nearby molecules during collisions. When a molecule undergoes a collision while simultaneously emitting a photon, the instantaneous energy maybe become slightly higher or lower depending on whether the molecule gains or loses energy during this instant. It can be shown that the effect of this slight energy transfer on average results also in a Lorentzian distribution with its own characteristic width [11].

In addition, the gas molecules are all moving with some velocity when at thermodynamic equilibrium. Because light that is emitted from a source moving towards or away from the observation point will undergo a shift of frequency (known as *Doppler shift*), light emitted in gas discharges will also be shifted in this fashion. Because molecules at thermodynamic equilibrium exhibit velocities determined by a Maxweillian distribution, the corresponding line profile resulting from this velocity shift will be Gaussian [11]:

$$f_G = \frac{1}{\sqrt{2\pi\xi^2}} e^{-\frac{(x-x_0)^2}{2\xi^2}} \tag{2.10}$$

where ξ is a parameter which determines line width. In spectroscopy, both pressure and Doppler broadening must be accounted for in simulation of emission peaks. The standard way of converting a theoretical spontaneous emission line of zero line width into the corresponding line profile is through the convolution integral:

$$f(x) * g(x) = \int f(y)\, g(x-y)\, dy \tag{2.11}$$

The basic process is as follows: first the emission line is determined from a Boltzmann distribution at temperature *T*, for a given energy transition with coefficient of spontaneous emission. Next this emission line of zero line width is multiplied by the convolution of Gaussian (Doppler) and Lorentzian (pressure) profiles and the line profile is determined. The convolution integral of these two profiles is known in literature as the Voigt function [11], and often the desire is to fit this Voigt profile (which is a function of the corresponding γ and ξ widths) to a measured emission line profile. This process is repeated for each line in the simulation range, which for this study is between 120 and 180 nm.

Note that the resulting calculated line profile would only be observed with a spectral instrument with infinite resolving power. In order to account for the aberration due to the spectrograph entrance slit and CCD pixel width, a rectangular line shape is also convoluted with the above profile. The effect of this rectangular profile is shown in Figure 2.4:

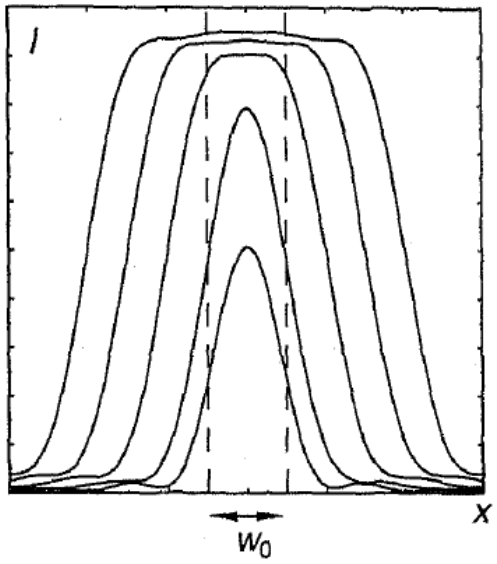

Figure 2.4: Effect of increasing rectangular slit width on calculated line profile [11].

2.4 VUV Absorption

A significant problem unique to spectral measurements of vacuum ultraviolet emission is the strong absorption of VUV light in most materials and gases. Indeed, vacuum UV is so named because it can only propagate long distances in vacuum environments, and in order to perform experiments in the VUV regime, it is required to select materials which are transmissive in the region of interest.

2.4.1 Absorption in Air

As discussed earlier, photons can be absorbed if they are captured by an electron which is able to make a transition into an excited or ionized state. In general this process can be described by an absorption coefficient (α) which relates the incident (I_0) and transmitted (I_T) intensities (Beer-Lambert Law):

$$I_T = I_0 \, e^{-\alpha(\lambda)x} \tag{2.12}$$

where x is the distance of material or gas the light must propagate through [13]. In general an absorption coefficient is wavelength dependent, and is usually a function of the cross section for the absorbing molecule or atom to interact with incident photons of a given energy (and thus wavelength).

Specifically of interest in this project, VUV light below 180 nm is highly absorbed in air at atmospheric pressure (see Figure 2.5). As noted in the figure, just 1 mm of air is enough to fully absorb VUV light in the range above 135 nm. A consequence of this absorption is that effective VUV studies must be performed under vacuum, in order to allow the distances required for correct focusing and imaging through an optical instrument such as a spectrograph.

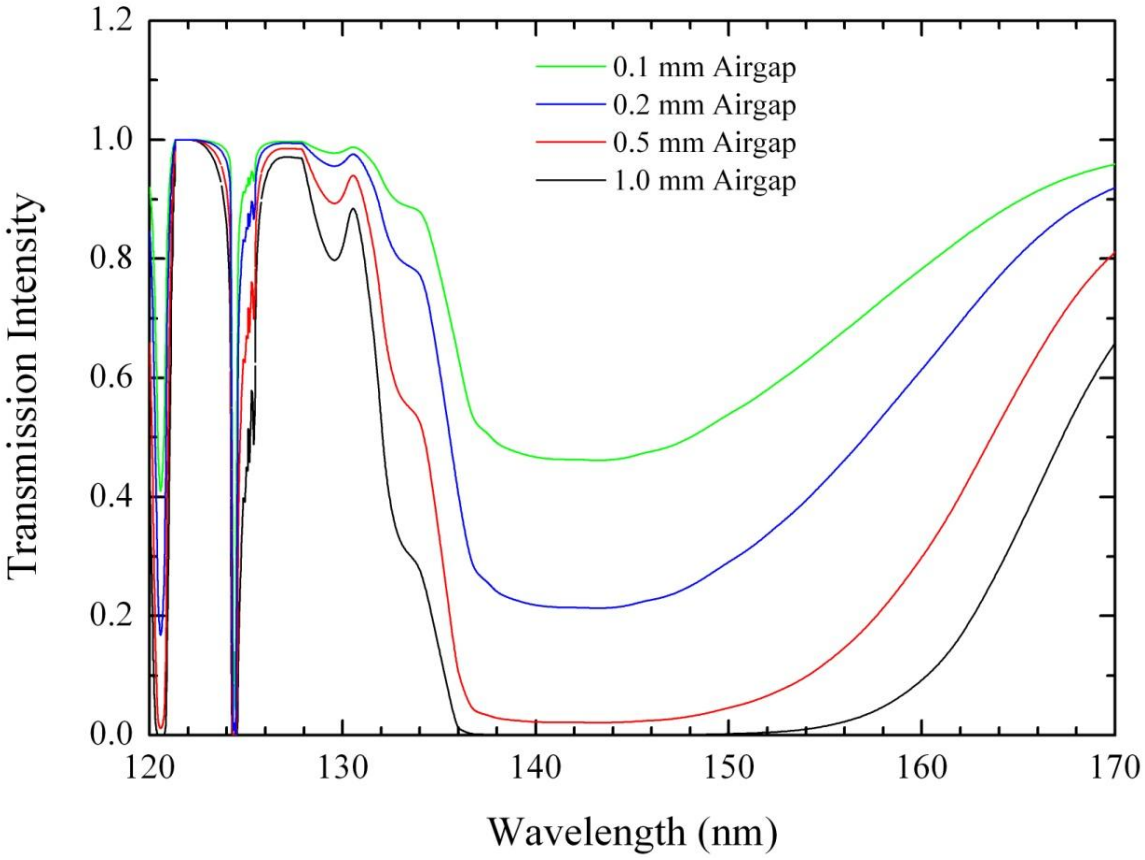

Figure 2.5: Transmission of VUV light in air for various air gap distances at 1 atm [9].

2.4.2 Absorption in Optical Materials

Because the phenomena of interest are atmospheric discharges and VUV instruments must be in vacuum to prevent absorption in air, a transition interface is required to separate the atmospheric and vacuum sides of the experiment. Normal glass is not transmissive to VUV light below 180 nm, and even fused silica used in other optical studies has a cutoff wavelength at 150 nm [9]. The fluoride materials such as lithium fluoride, magnesium fluoride, and calcium fluoride are standard materials used for vacuum UV transmission [10].

Because this study is of atmospheric discharges, magnesium fluoride was chosen because of its hardness as compared to the other fluoride glasses, which helps resist material erosion during the discharge process. The band gap of magnesium fluoride is 10.8 eV, which corresponds to a wavelength of around 115 nm [9]. Thus, magnesium fluoride will transmit VUV light down to this wavelength, where photons with wavelengths shorter than 115 nm will have sufficient energy to excite MgF_2 valence electrons into the conduction band. The supplied transmission curve for magnesium fluoride is shown in Figure 2.6 (for 10 mm sample thickness):

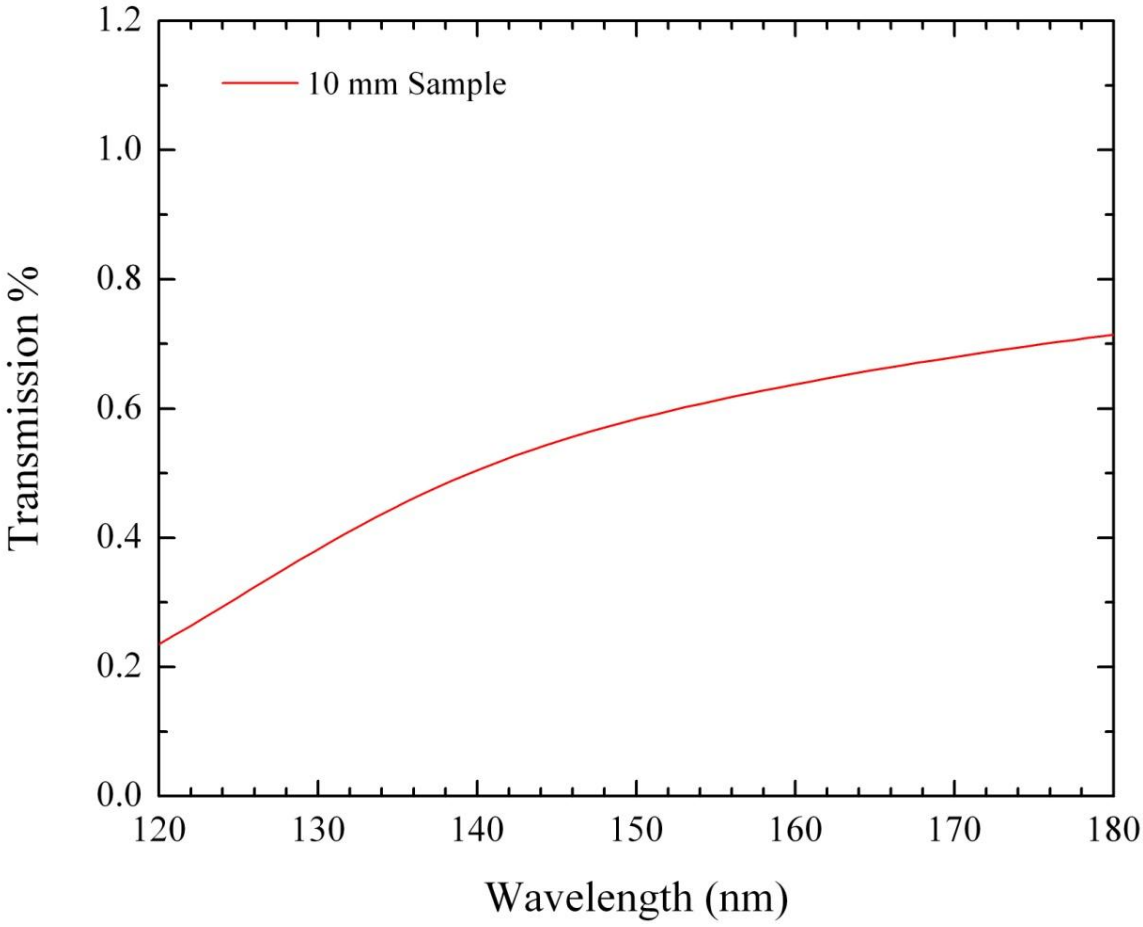

Figure 2.6: Transmission of VUV light through 10 mm of MgF_2 [10].

The absorption (or *extinction*) coefficient can be calculated from this supplied transmission curve for the given test thickness with Equation 2.12, which will later allow the calculation of the exact influence of MgF_2 on an experimental apparatus with multiple MgF_2 components (see Figure 2.7):

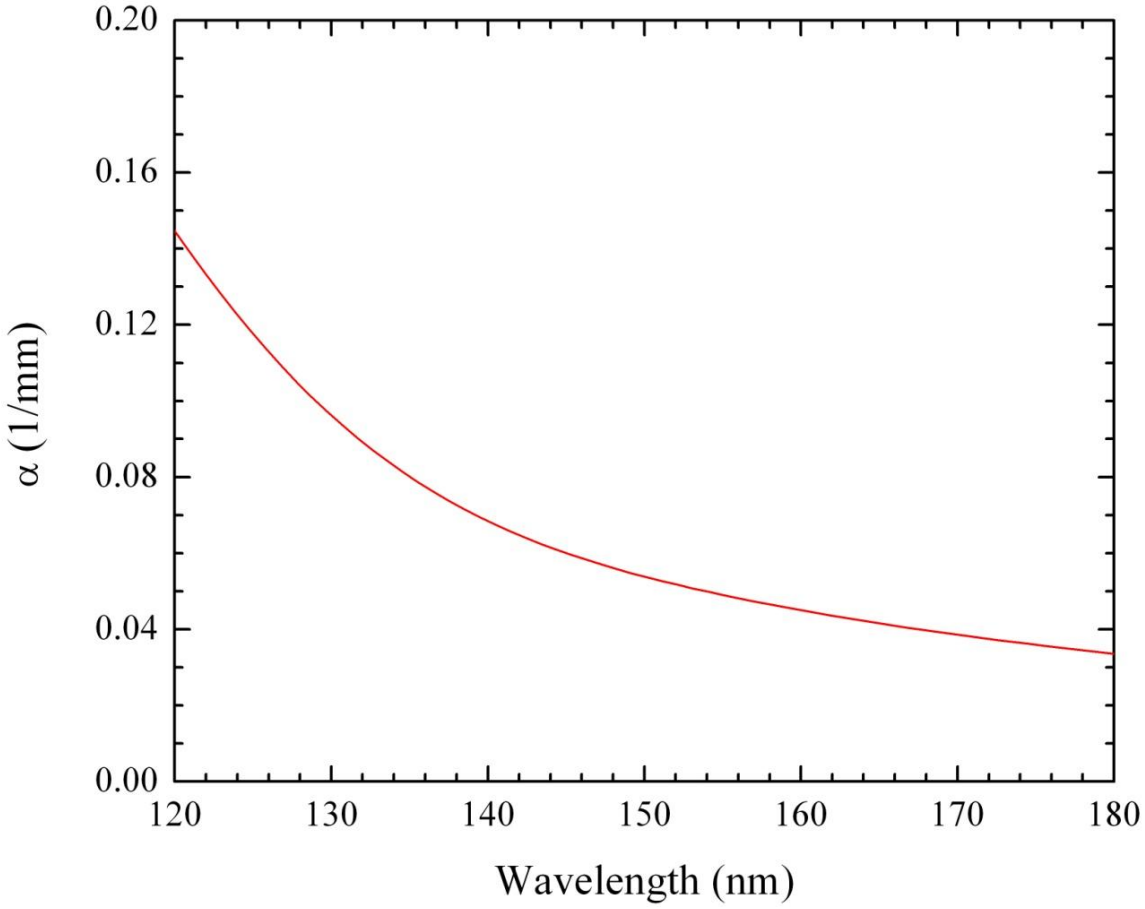

Figure 2.7: Calculated absorption coefficient for MgF_2 in the VUV range.

2.5 Previous Research

The physics of surface flashover have been extensively studied at the Center for Pulsed Power and Power Electronics at Texas Tech University for the past 20 years, and the current research is a result of previous iterations of successful programs. Of specific interest in the study of VUV physics from atmospheric discharges are previous breakdown projects concerning UV radiation and early VUV emission measurements of flashover.

2.5.1 HPM Window Flashover

Almost all of the flashover physics research at TTU is targeted towards the understanding of breakdown which occurs on the interface between atmosphere and vacuum of certain high power systems [17-19], for example on the transition of high power microwave (HPM) generators [20]. When the microwave pulse is generated in vacuum, it is channeled into the atmosphere and must pass through a window surface which separates atmosphere from vacuum. As the local electric field grows when the microwave propagates through the window, free electrons can form avalanches and cause a breakdown event along the surface. The bulk breakdown avalanche can form a plasma sheath that can reflect the incoming microwave power, which is partially absorbed or directed back into the generator and can damage sensitive electronics [21].

It was shown in previous studies of HPM surface flashover that external UV excitation decreased the delay time for induced breakdown trials [22]. Spectral

measurements from surface flashover events showed that microwave induced plasmas contained limited oxygen emission in the UV to visible range, see Figure 2.8:

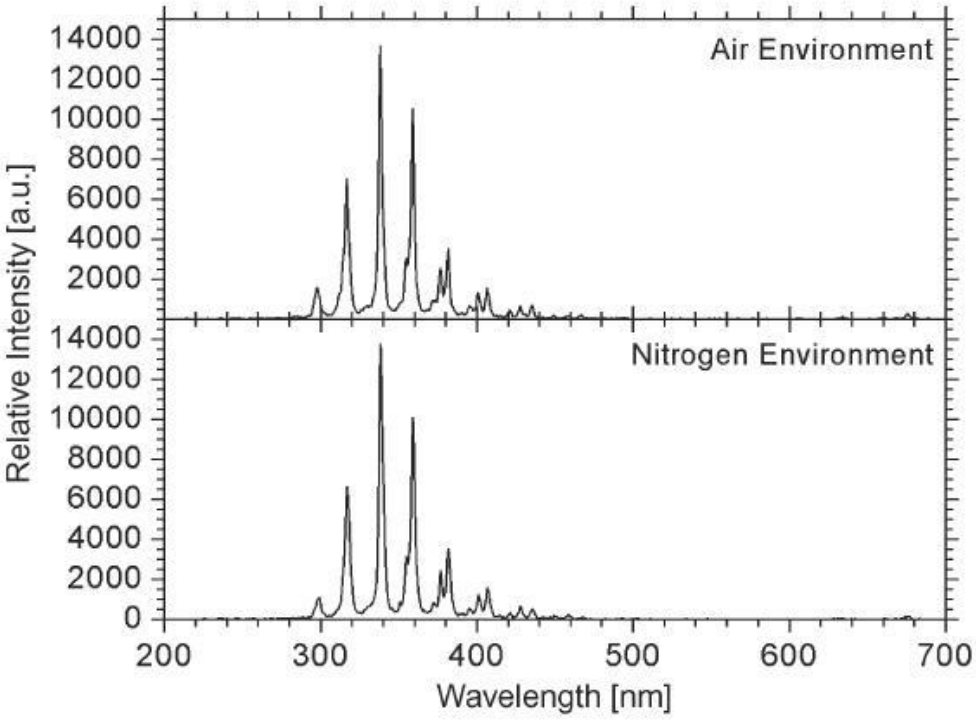

Figure 2.8: Emission from HPM breakdown in air and pure nitrogen environments [22].

Note that the emission is largely similar between air and pure nitrogen environments, which indicates limited emission of other gas molecules such as oxygen and argon during breakdown. However, it was suggested that the limited emission is due to microwave power being reflected during breakdown, and thus the temperature of the discharge would be low. This would lead to fewer emissions of UV photons from processes discussed in Section 2.3, especially from oxygen molecules which are prevalent in the atmosphere and could contribute to breakdown because of the strong absorption of UV radiation by oxygen molecules [9].

2.5.2 Unipolar Flashover

It was shown that similarities exist between HPM and some high power unipolar breakdown events [23]. For example, if the unipolar electrode tips are inserted into the dielectric surface, the DC electric field can be matched to a similar peak RF field observed from a high power microwave passing through the surface [22]. Previous studies of unipolar breakdown events suggested that higher temperature discharges contain a number of oxygen emission modes in the UV range (see Figure 2.9):

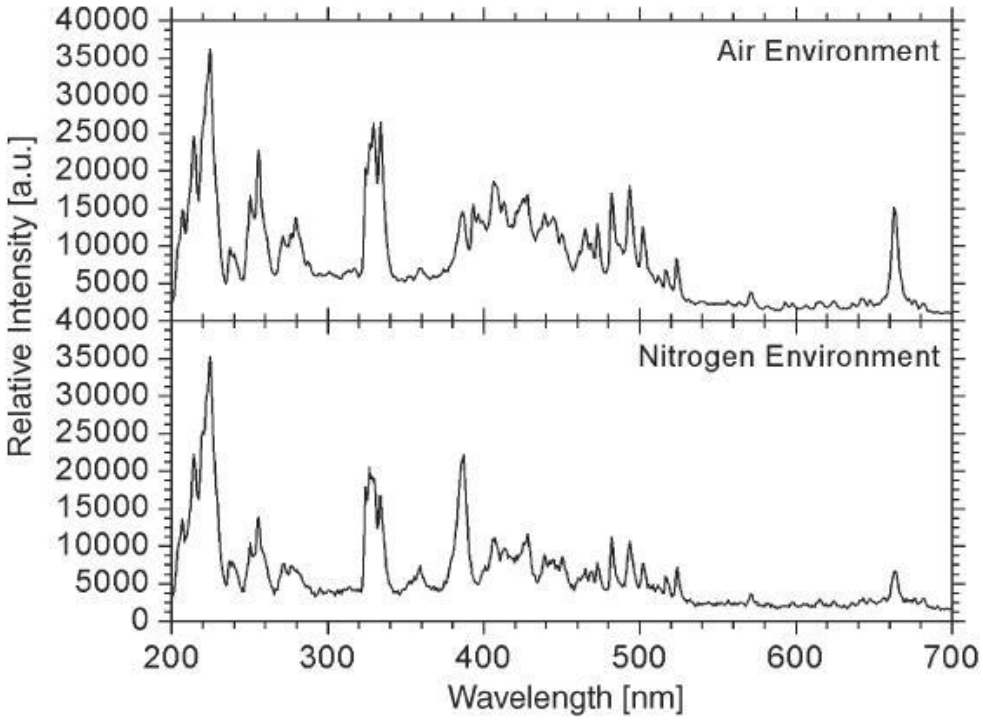

Figure 2.9: Emission from unipolar breakdown in air and pure nitrogen environments [22].

This would at least intuitively suggest that an investigation at lower wavelengths would unveil oxygen emissions that could significantly contribute to atmospheric breakdown, but due to instrument limitations these studies were only sensitive down to 200 nm. Thus it was decided that a new experiment is needed which could investigate unipolar flashover events related to HPM breakdown, yet have the capability of investing the emission of vacuum ultraviolet light.

2.5.3 Early VUV Studies

A first generation setup was designed which could extend the UV detection range of emission diagnostics for unipolar discharges [9]. The setup basically consisted of a vacuum spectrograph which focused light from an excited flashover event onto a window coated with a scintillating material. This material absorbed UV photons and re-emits photons in the blue part of the visible spectrum, which is easily detected by standard ICCD systems. An example of emission states which were observed in this study are shown in Figures 2.10 and 2.11. It was concluded that while some VUV emission was present in the discharge, a more advanced apparatus is required which can resolve VUV emission in the key excitation range from 120 into 180 with good signal-to-noise ratio, high reproducibility, and accurate time resolution.

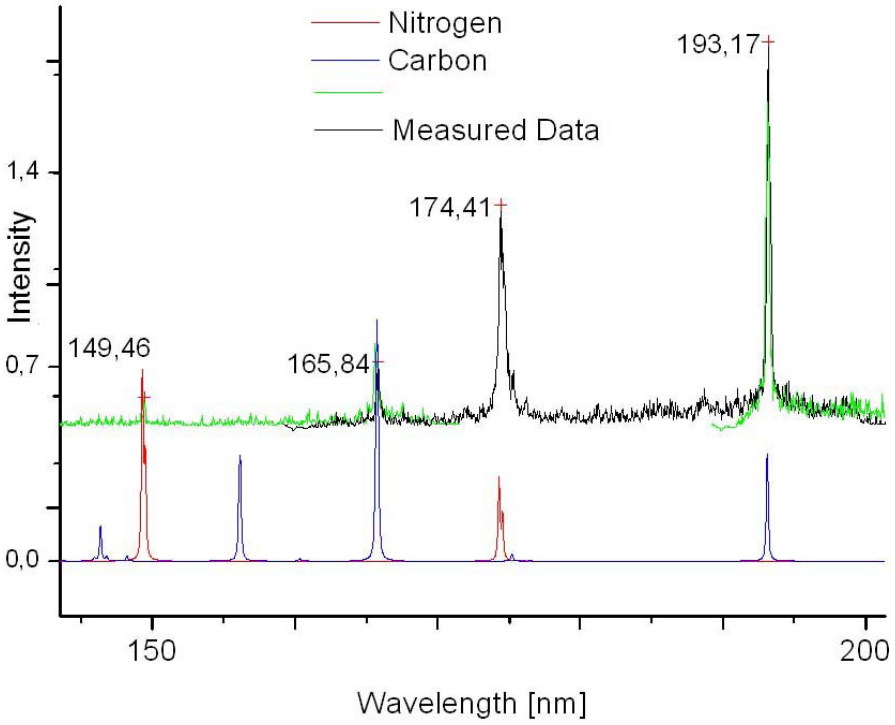

Figure 2.10: VUV emission from an atmospheric discharge, with spectral simulation [9].

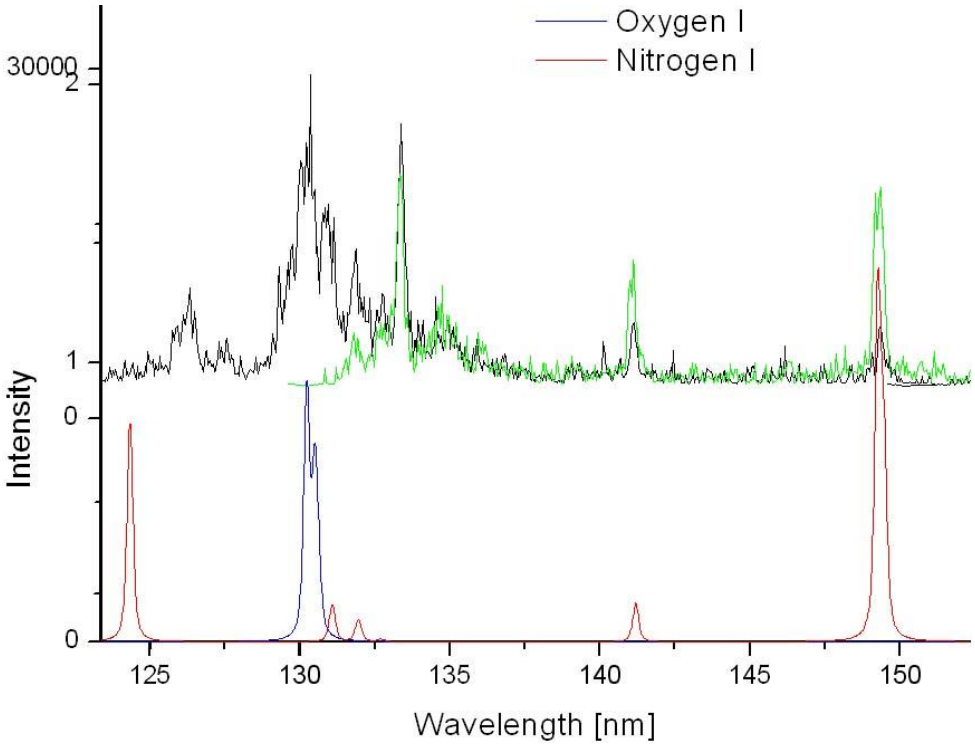

Figure 2.11: VUV emission from an atmospheric discharge, with spectral simulation [9].

CHAPTER 3

EXPERIMENTAL SETUP

It was desired to study the emission from dielectric surface flashover, specifically to quantify the role of VUV radiation in the development of fast pulsed breakdown in atmosphere. An experiment was constructed that basically consists of a repetitive high voltage pulser which excites a surface flashover event across a window dielectric under controlled atmospheric conditions [24]. The self emission of this plasma is focused by means of VUV transparent optics into a vacuum spectrograph, and is detected either by ICCD or photomultiplier electronics. In addition, high temporal resolution optical imaging (with gate times smaller than 3 ns) coupled with detailed electrical and emission diagnostics of breakdown allow for complete reconstruction of the flashover event with nanosecond timescales. An overview of the experimental setup is given in Figure 3.1:

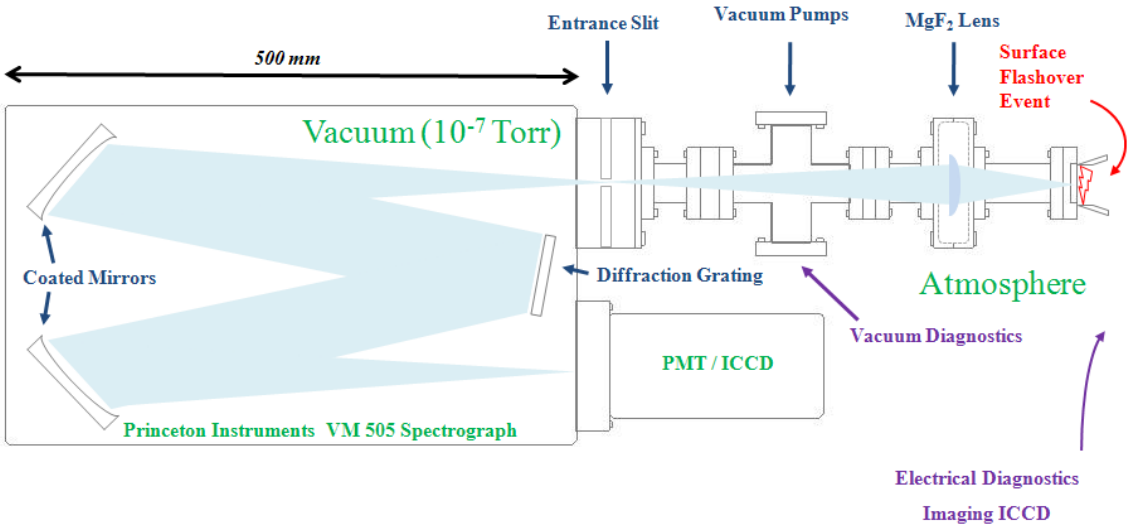

Figure 3.1: Experimental setup to study VUV emission from surface flashover [24].

3.1 Flashover Environment

The experimental setup is designed so that VUV emission from an excited surface flashover event is focused onto the entrance slit of a vacuum spectrograph, with the spark simultaneously being imaged through a fast shutter ICCD on the atmospheric side. The entire flashover gap is contained in a Lexan chamber (see Figure 3.2), which enables flashover testing in diverse gases and gas mixtures at atmospheric pressure. When a particular gas is desired in the test chamber, the outside window is attached and a positive pressure is applied to the chamber with flowing gas. It is not necessary to use a steel flange for this procedure, and after around 30 seconds the chamber is completely filled with the target gas when under a light flow. When flammable gases were used, a thin layer of aluminum foil was used instead of the mounted external window so the foil can be easily ejected if combustion occurs during flashover, preventing shrapnel damage to the laboratory. A secondary quartz window was inserted into the window chamber, allowing for a triggerable ICCD system to image the flashover event from the atmospheric side.

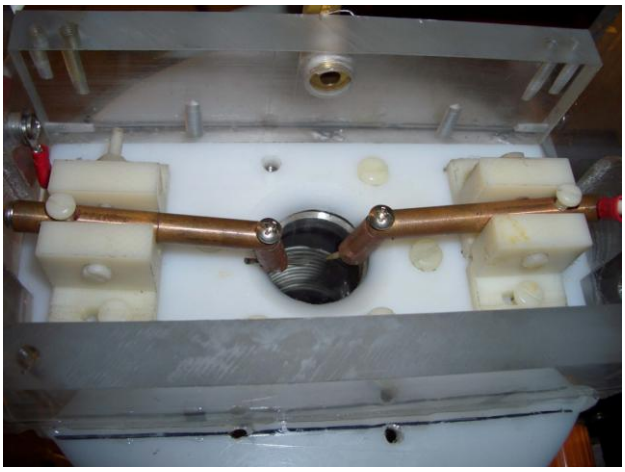

Figure 3.2: Lexan gas chamber and electrodes for surface flashover studies.

3.1.1 Electrode Geometry

The electrode setup was chosen to maximize streamer production from the triple point between metal, air, and dielectric. Sharpened stainless steel electrodes (estimated tip radius of 200μm) are attached to springs which press down onto a MgF_2 surface a distance of 8 mm apart (see Figure 3.3). Stainless steel was used because it was shown that copper electrodes leave a thin layer of sputtered copper on the window surface after just a few shots [9]. The electrodes are positioned so that the spark develops perpendicular to the entrance slit of the spectrograph, in the horizontal plane. By doing this, the positional jitter from the spark is negligible and the "center" part of the spark will always pass through the entrance slit of the spectrograph. If this is not done and the electrodes are mounted vertically, the spark may jitter by as much as a millimeter, and the focused spark sometimes lands outside the entrance slit, causing a large shot-to-shot uncertainty in the emission diagnostic.

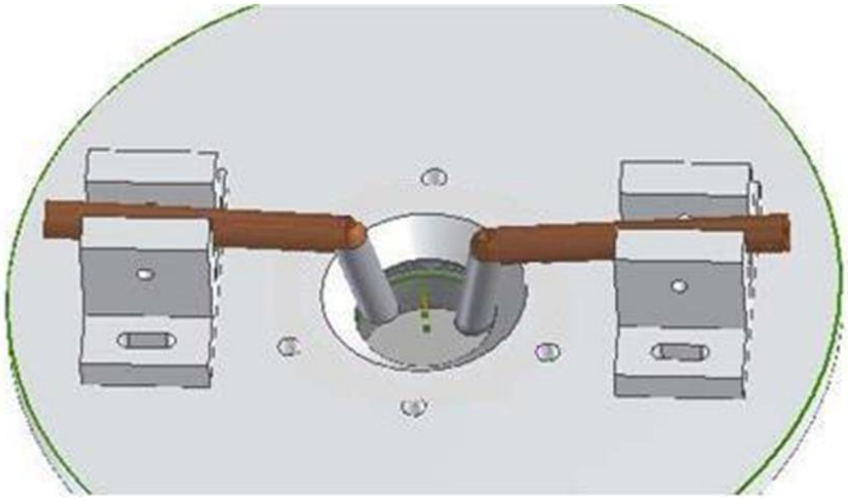

Figure 3.3: Electrodes resting on the MgF_2 surface [9, 24-25].

3.1.2 Window Dielectric

As discussed previously, Magnesium fluoride (MgF_2) was chosen as the window dielectric since it is VUV transmissive down to its cutoff wavelength of around 115 nm. The window used was 38 mm in diameter with a thickness of 5 mm. This thickness was chosen to hold off a pressure difference between vacuum and atmosphere at this interface (t = 3 mm from calculation, but 5 mm was chosen for safety). From theory [9], the required window thickness can be determined with parameters given in Table 3.1:

$$t = \sqrt{\frac{0.5\, A_w\, K\, f_S\, \Delta P}{S_F}} \tag{3.1}$$

Table 3.1: Parameters which are used to calculate the flashover dielectric window thickness.

Parameter	Value
Pressure Differential (ΔP)	1.0 Atm
Window Diameter (d)	38 mm (ConFlat®)
Aperture Size (A_w)	1135 mm^2
Safety Factor (f_S)	3.5 - 4.0
Yield Strength (S_F)	33 Mpa (glass)
Clamping Constant (K)	1.25 (Unsupported)

Unfortunately, since the repetition of triggered spark events on the surface causes erosion of the material, the MgF_2 window must be cleaned or replaced every few hundred shots to allow for consistent optical properties. During this process the window is removed from the experiment, polished with descending grits down to ¼ micron fineness, and then carefully cleaned with cyclohexane [24]. Figure 3.4 shows the before and after result of this cleaning process.

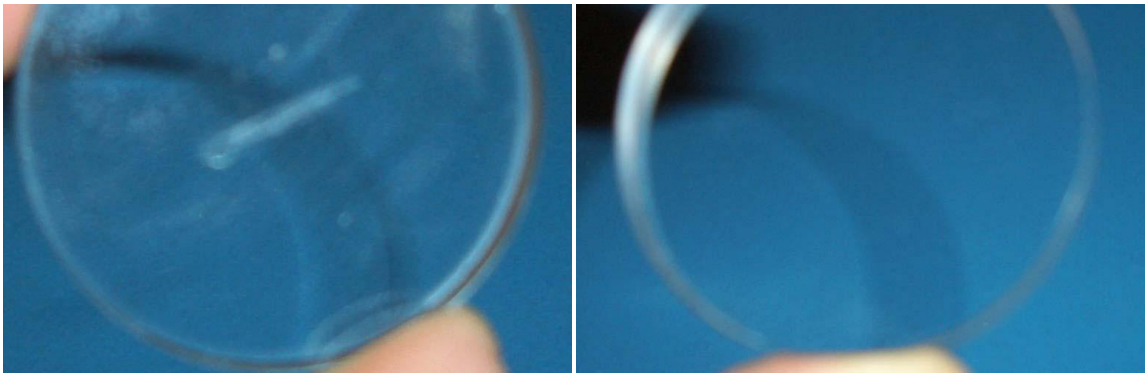

Figure 3.4: MgF_2 surface (a) before and (b) after cleaning procedure [9].

3.2 High Voltage Pulser

Utilizing an externally triggerable solid-state pulser, a high voltage pulse is applied to the flashover electrodes [25-26]. The essential circuit scheme basically consists of a capacitor charged to a few kV which is switched into a pulse transformer, and is outlined below in Figure 3.5:

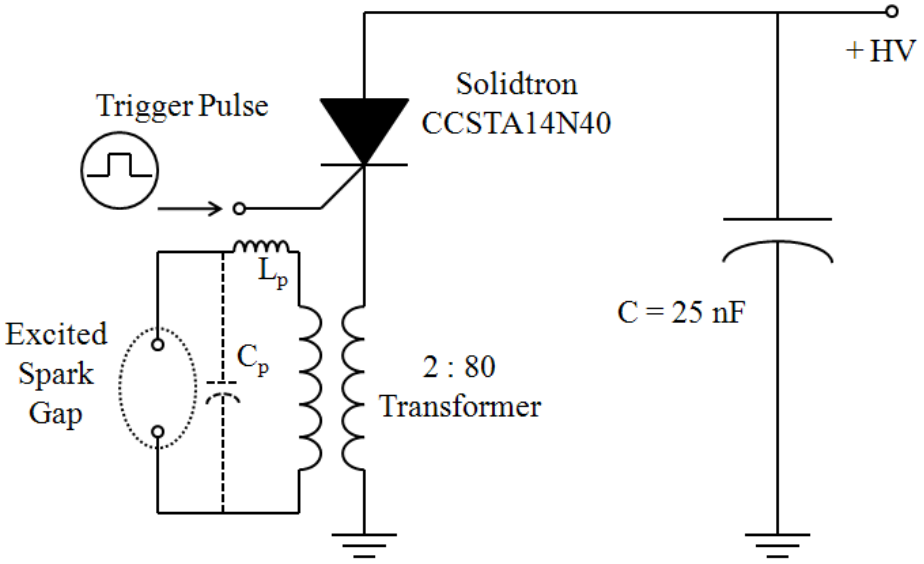

Figure 3.5: High voltage circuit used to produce excited surface flashover events [24].

The original pulser used in this project contained a hermetically sealed miniature trigatron spark gap, Perkin Elmer GP-489, as the primary switch [26]. Unfortunately the lifetime of these gaps proved to be less than roughly 2000 shots, which was a significant issue since (at that time) a single data set for VUV spectroscopy occasionally reached 100 shots or more. Post mortem analysis of the switch showed coating on the inside of the spark gap envelope presumably due to ablated electrode material.

As a precautionary measure to extend the pulser lifetime, the trigatron spark gap was replaced by a solid state switch, while the primary circuit topology remained the same [25]. The switch used for the upgraded pulser design was the CCSTA14N40 thyristor by Solidtron / Silicon Power. This switch is rated at 4 kV with a repetitive peak current of 10 kA when in pulsed operation [27]. While the design of the switching scheme consisted of a target repetition rate of 10 Hz, typical VUV producing flashover events are only triggered at a rate of 1 Hz.

The secondary of the step-up transformer (2:80 ratio) with Metglas® core (2.05 cm^2 cross sectional area) is directly connected to the flashover gap. The voltage on this secondary can range from 20 kV to 50 kV as a function of charging voltage between 2 to 4 kV. Sufficient VUV emission is observed when the gap is allowed to flash over while overvoltaged, with a peak voltage of typically 22 kV and a circuit limited current of 35 A with low temporal jitter. Typical voltage pulses have a FWHM pulse-width of 500 ns and 10 - 90% risetime of 100 ns.

3.3 Optical System

The primary diagnostic tool used in this study is time resolved emission spectroscopy, and so a detailed optical system was conceived to measure the VUV emission from a surface flashover event. A primary concern is the absorption of VUV light in common optical materials, and as a result, a number of design constraints were introduced into the system.

3.3.1 Light Path

In order for the flashover event to be correctly imaged into the entrance slit of the spectrograph, an optical pathway of steel tubing is required to increase the overall light path length and match the focal distances of the optics. A lens must be used to focus an 8 mm spark into a 4 mm entrance slit, and the distances along this optical path were chosen so as to match the F number of the spectrograph which will correctly reproduce the spark's image in focus. Because of concerns for absorption of VUV in common optical materials, MgF_2 was chosen as the lens material because it is transmissive down to its cutoff wavelength of 115 nm. However because MgF_2 has a varying index of refraction below 300 nm, the resulting focal length will also be a function of wavelength in this range. The index of refraction of MgF_2 was approximated by a 3^{rd} order Sellmeier equation (where the coefficients have been tabulated in literature [28]), see Figure 3.6:

$$n = \sqrt{1 + \frac{C_1\lambda^2}{(\lambda^2 - {C_2}^2)} + \frac{C_3\lambda^2}{(\lambda^2 - {C_4}^2)} + \frac{C_5\lambda^2}{(\lambda^2 - {C_6}^2)}} \tag{3.2}$$

Table 3.2: Coefficients for the Sellmeier equation used to calculate the index of refraction for MgF_2 [28].

Sellmeier Coefficient	Value
C_1	0.48755108
C_2	0.04338408
C_3	0.39875031
C_4	0.09461442
C_5	2.3120353
C_6	23.793604

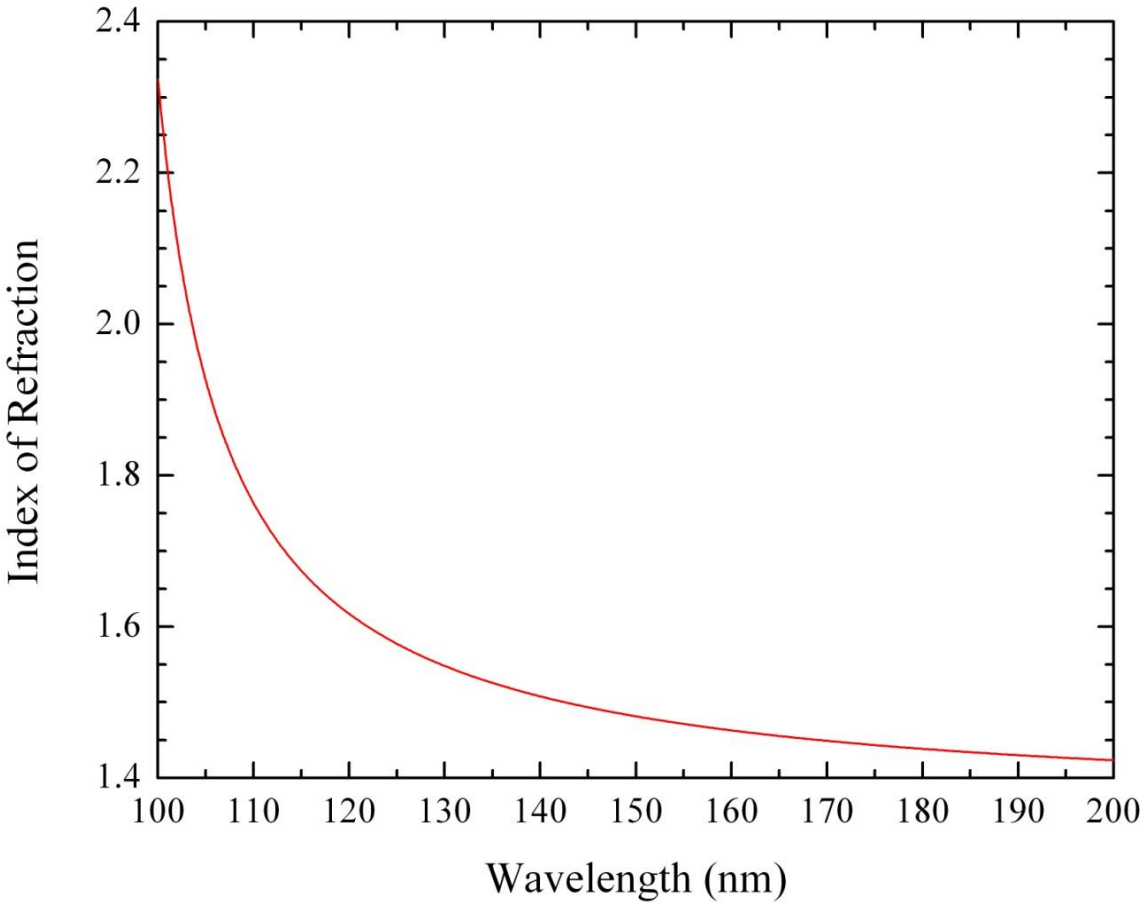

Figure 3.6: Calculated index of refraction of MgF_2 in the VUV range.

After the index of refraction is known, the focal length of a plano-convex lens can be determined by the lensmaker's equation, where the index of refraction for vacuum (n_{vac}), the incident radius of curvature (R_1), and the exit radius of curvature (R_2, assumed to be infinity for plano-convex) are known [29]. The lens used in this experiment has an incident radius of curvature of 49 mm, and the resulting focal length is shown in Figure 3.7:

$$\frac{1}{f} = \frac{n - n_{vac}}{n_{vac}} \left(\frac{1}{R_1} - \frac{1}{R_2} \right) \tag{3.3}$$

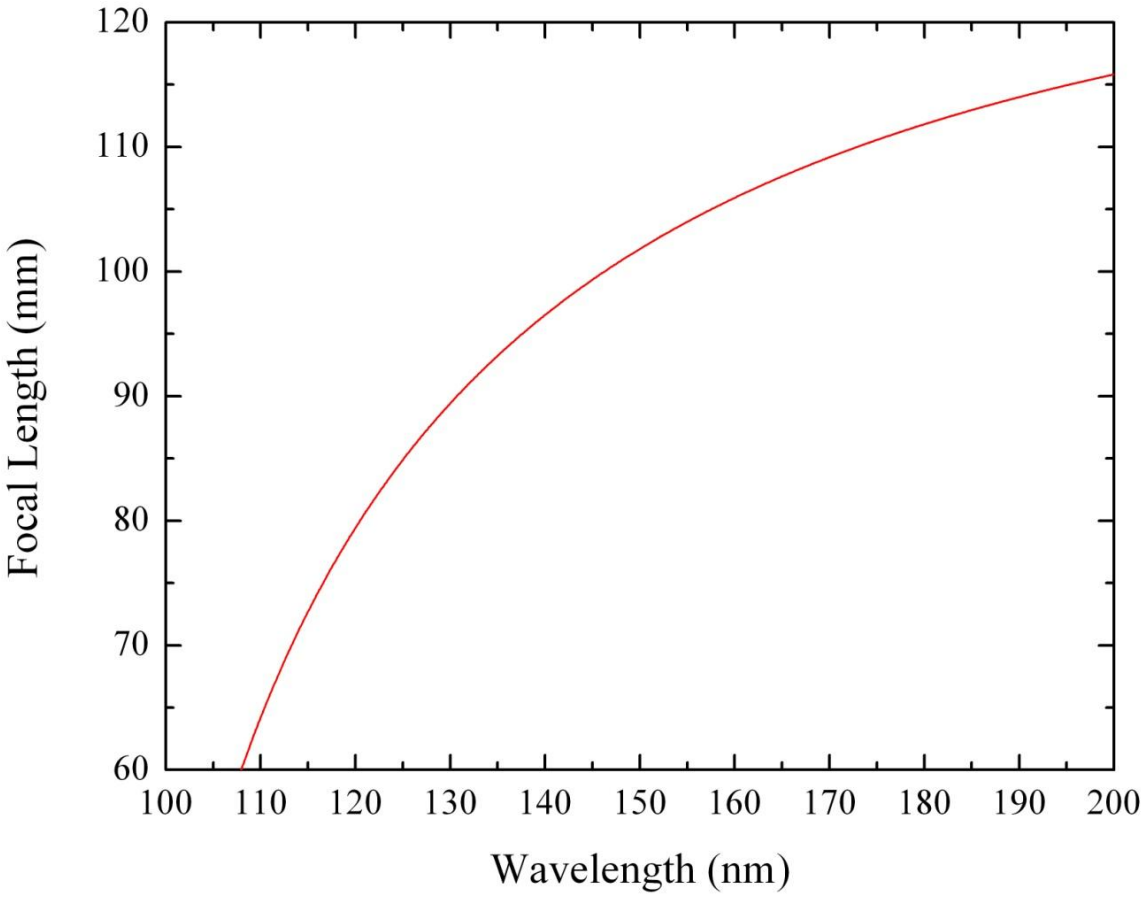

Figure 3.7: Focal length of the MgF_2 lens in the VUV range.

Because of this varying focal length, the light path was designed to allow for stainless steel ConFlat® spacers to be inserted in the section between the lens and entrance slit to keep the F numbers matched for a given target wavelength for a particular measurement. The exact path lengths which would accurately perform a ½ magnification of the spark

were determined through the use of Optical Ray Tracer, an open source optics design suite [30]. The relevant parameters for the optical system are shown in Table 3.3.

Table 3.3: Calculated parameters for the optical system which focuses the spark into the spectrograph.

Parameter	Value
Lens Focal Length (*f*)	89.4 mm
Optimized Wavelength (λ)	130 nm
Spectrograph Focal Length	500 mm
Spectrograph F - Number	8.7
Object - Lens Distance (x_o)	120 mm
Lens - Image Distance (x_i)	300 mm

Because the optical section needs to be kept under vacuum (10^{-7} Torr) for VUV propagation, a turbo pump / oil free membrane roughing pump pair is mounted along this vacuum path length. A hole was removed in the optical table so that the pumps can rest under the experiment and reduce vibrations from pumping. Because the entrance slit has a manual valve which can separate the optical path from the spectrograph chambers, it is possible to remove this vacuum section while the spectrograph remains evacuated, and vice versa. This is so the optical materials, which can absorb moisture from the atmosphere and accumulate imperfections, can remain under vacuum at almost all times. Electronic vacuum gauges are mounted at the connections for the pumps.

3.3.2 Spectrograph

The spectrograph used in this study was the vacuum monochromator VM-505 by Acton Research Corporation (now Princeton Instruments). This spectrograph has a focal length of 500 mm (F - number = 8.7), with adjustable entrance and exit slits from 10 µm to 2 mm. The spectrograph mirrors have been coated with a proprietary Aluminum – MgF_2 composite (#1200), which provides an effective reflectance of 82% at 120 nm (see Figure 3.8) [31].

The spectrograph grating used has an effective area of 52 x 52 mm, with 1200 Grooves / mm which has been blazed for 150 nm. This gives a reciprocal linear dispersion of nominally 17 Å/mm in first order [9]. The grating is tuned by a high precision step motor, which is digitally controlled by the Spectradrive Controller SD-748. For measurements, the spectrograph grating is always positioned at the shortest wavelength and then scanned through to the longest wavelength in the study (for example, from 120 to 180 nm). This is because the Spectradrive controller always turns "into" the longer wavelength, so if the experiment were to start from a longer wavelength and end at a shorter wavelength, the Spectradrive has to do more work during this process which may introduce small errors in the grating angle.

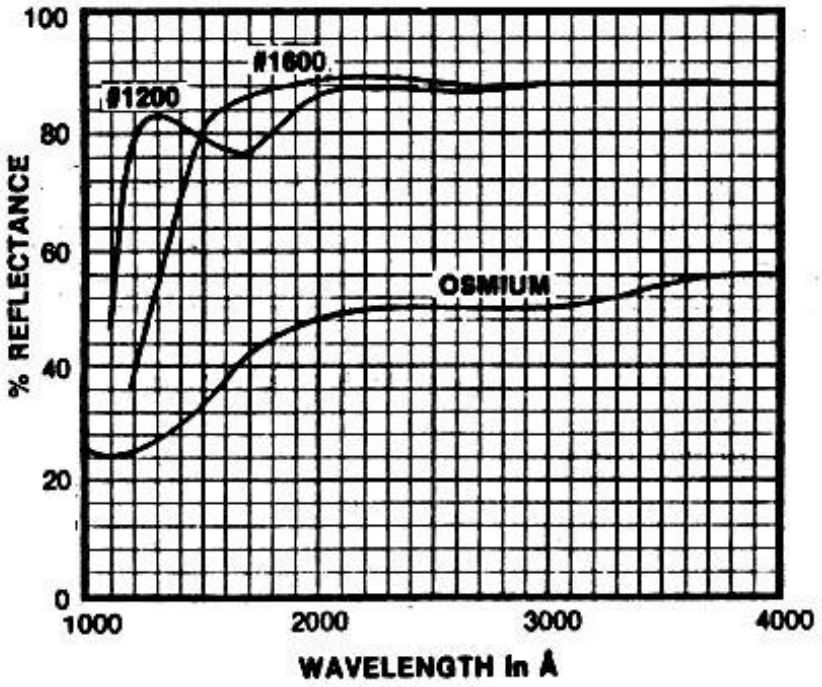

Figure 3.8: Reflectance of spectrograph coatings in the VUV range [31].

The spectrograph is also mounted with its own turbo / roughing pump pair. A section was cut into the optics table so the turbo pump can hang mounted from the bottom of the spectrograph. When adjustments inside the spectrograph are required, a valve is closed to the roughing pump and the turbo pump is allowed to wind down without power. Moisture free gas is then flowed into the spectrograph so the optics remain somewhat protected and lifetime increased. A vacuum gauge is mounted in series between the turbo and roughing pump, so the vacuum inside the spectrograph can be estimated at least as good as the gauge reading indicates. For typical measurements, the vacuum for this experiment is held constant at roughly 10^{-7} Torr.

3.4 Diagnostics

Because the goal is to observe VUV activity emitted from electrical breakdown, it was required to design a diagnostic scheme which will monitor electrical characteristics of breakdown and corresponding optical emission with timescales on the order of nanoseconds. As a result, a typical trial consists of voltage and current measurements, ICCD or photomultiplier emission diagnostics in the VUV regime, and high resolution gated optical imaging. A diagram of the general diagnostic scheme is shown below in Figure 3.9:

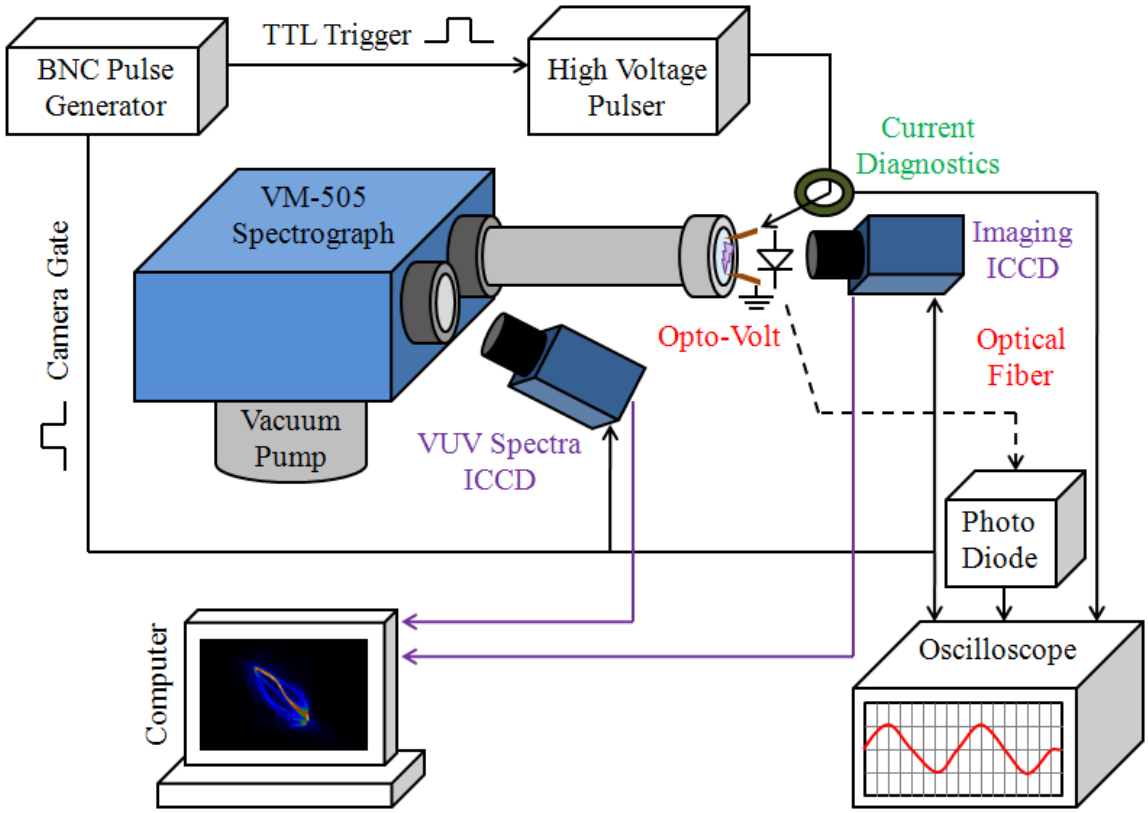

Figure 3.9: Block diagram of the diagnostic setup used in this study.

3.4.1 Electrical Diagnostics

Electrical diagnostics can provide insight into the instantaneous change of voltage and current during the breakdown process, and can be used to supply a timescale for optical diagnostics. Current diagnostics include a Rogowski type probe and a Pearson™ Electronics model 2878 current probe, which has a useable rise time of 5 ns and sensitivity of 0.1 Volt / Amp [32]. The Rogowski probe was used for increased dynamic range during the fast time scales of streamer propagation, and general Rogowski probe characteristics are discussed in Appendix A.

For spark gap voltage diagnostics, a custom optically isolated probe was constructed from a laser diode in series with a 2 MΩ resistance. When this device is placed across the spark gap with high voltage, very little current (on the order of milliamperes) conducts through this circuit while most current still passes through the gap during breakdown. The small current is enough to drive the laser diode, and the light output (which is somewhat proportional to the applied voltage) passes through a fiber to an isolated photodiode whose output is recorded. The result is a comparatively noise free high voltage diagnostic for pulsed breakdown studies with a somewhat non-linear response, with an estimated 10% accuracy and high repeatability [24]. Note that this method provides a differential voltage measurement (a ground reference is not required) and enables measuring gap voltage with very short leads, greatly reducing the inductive voltage drop always affecting pulsed voltage measurements with fast current changes. All electrical diagnostics are recorded by high bandwidth oscilloscopes (1 GHz, 4 GSa/s) in shielded screen-rooms for noise reduction.

3.4.2 Spectroscopy

The exit slit of the spectrograph can be mounted with either ICCD or photomultiplier diagnostics. For the detection of VUV light, careful thought was given to the choice of optics used to prevent absorption below 180 nm. For photomultiplier detection, the R8486 side-on PMT from Hamamatsu Corporation was used. The PMT features a MgF_2 entrance window for VUV transmission, and Ce-Te photocathode (20% quantum efficiency below 200 nm, <5 ns rise-time) for VUV sensitivity [33]. This PMT was baked into a custom compression fitting and mounted into a standard CF-450 flange by the manufacturer. A modified T-bracket flange was constructed in the P3E center which holds the sensitive side-on area of the PMT outside the exit slit of the spectrograph. As an optical alignment procedure, a low power green laser is sent into the optical pathway and focused through the spectrograph into the PMT unit which is covered by a small piece of Teflon tape to prevent damage from overexposure to the PMT photocathode.

The photomultiplier provides a temporally continuous VUV emission readout, which is converted into a voltage signal and recorded by an oscilloscope. Significant shielding is used around the PMT, power supply casing, and battery to reduce noise in the recorded PMT signal. When PMT measurements are made, the spectrograph exit slit is closed to 20 μm so only the center line (within 70 pm) is allowed into the PMT. The Spectradrive controlled grating is then scanned through multiple shots at 0.1 nm steps through the target wavelength range.

For ICCD analysis of spectra, the DH740 series camera from Andor™ Technology is used. This ICCD also features a MgF_2 entrance window for VUV transmission, and high shutter speed for time resolved spectroscopy (13% quantum efficiency with minimum 2 ns gate) [34]. This camera comes pre-installed with an 18 mm diameter E2V model CCD42-10 chip with 2048 x 512 resolution with effective pixel size of 13.5 μm^2. This camera has a peltier element that cools the CCD to -15° C which reduces thermal noise. For these studies the ICCD is triggered by a square pulse from a delay generator by Stanford Research Systems.

For complete recording of VUV emission throughout the entire discharge, the camera is gated for 2 μs which captures the majority of the discharge activity. If time resolved spectroscopy is desired, the camera is gated for 100 ns intervals during the period before and after voltage collapse, which provides information of VUV activity for these periods only. The CCD is then digitized and sent to a computer controller card for analysis in the Andor™ Technology SOLIS software. The digitized data is later vertically binned in this software, which results in simple (x. y) coordinate pairs of spectral activity.

When the ICCD is used, the exit slit of the spectrograph is removed and the focal plane of the spectrograph is exposed to the CCD. As a result, the spectral range of a single measurement is around 25 nm and the dispersion must be calibrated. During this process, a known emission line from flashover is measured with the Spectradrive in two consecutive positions, and the change in Spectradrive wavelength can be used to calculate the dispersion from the pixel shift observed in the software.

3.4.3 Imaging

The final diagnostic discussed in this flashover setup is optical imaging of the flashover event, as seen from the atmospheric side of the window dielectric. The purpose of this diagnostic is to visually compare the changes in electrical and emission diagnostics to the changes in observed streamer activity. As stated before, the Lexan flashover chamber contains a quartz window port which an outside ICCD camera can image through.

For this study, the camera used for imaging is the DH734 series ICCD from Andor™ Technology (quantum efficiency of 16% in the optical range, minimum gate time of 2 ns) focused by a UV-Nikon 105 mm f/2.8 Micro lens [35]. This camera features a 25 mm diameter Marconi CCD47-10 chip with 1024 x 1024 resolution with effective pixel size of 19.5 μm^2. For typical flashover events, this camera is gated for 3 ns with high gain, and the internal digital delay generator (DDG) delay time is controlled to scan through different periods of the discharge. This camera will capture optical emission from flashover in the range between 180 and 850 nm, which corresponds to primarily the visible light spectrum.

Because the intensifier gain is logarithmically controlled, it is possible to scan through discharge periods which can span multiple orders of magnitude in luminosity. Typical shot-to-shot jitter for breakdown can be as high as 10 ns, so a single DDG delay position may result in images corresponding to a number of different breakdown stages. Also note that in this method it is not possible to image a single discharge many times

because the camera is only used for single shot imaging, but through the reconstructive system of electrical diagnostics and due to high repeatability of the flashover events, it is possible to create a series of images which show streamer activity in each major period before full voltage collapse.

CHAPTER 4

EXPERIMENTAL RESULTS AND DISCUSSION

4.1 Lamp Calibration

The first step in accurately understanding the emission from surface flashover is to map the experimental profile of our optical apparatus. The optical system is inherently lossy in the VUV regime because of absorption in MgF_2 materials, so it is necessary to use a broadband calibration lamp to quantitatively measure this loss. For this procedure, the L7293 model lamp from Hamamatsu Corporation is used. This lamp contains a glow discharge in deuterium gas which produces a broad spectrum in the VUV range (see Figure 4.1) [36].

4.1.1 Measured Experimental Profile

The broad spectrum VUV lamp was used to measure the experimental profile by allowing the lamp's emission to propagate through the optical system. The lamp is mounted so the tip of the glass head (which contains a MgF_2 exit window) rests against the MgF_2 input window of the light path. Note the lamp produces a rather intense luminosity of UV radiation, so a black cloth is placed over the lamp to limit exposure to students nearby in the laboratory. The emission from the lamp is recorded by the ICCD camera mounted at the exit plane of the spectrograph. For these measurements, the camera accumulates 30 sets of 1 ms gates with low gain at 20 nm intervals. The

normalized result of this measurement is given in Figure 4.1 and compared to a base curve supplied from the lamp's manufacturer. As expected, the majority of measurement is in agreement except for the region below 130 nm, which largely corresponds to the absorption loss from MgF_2.

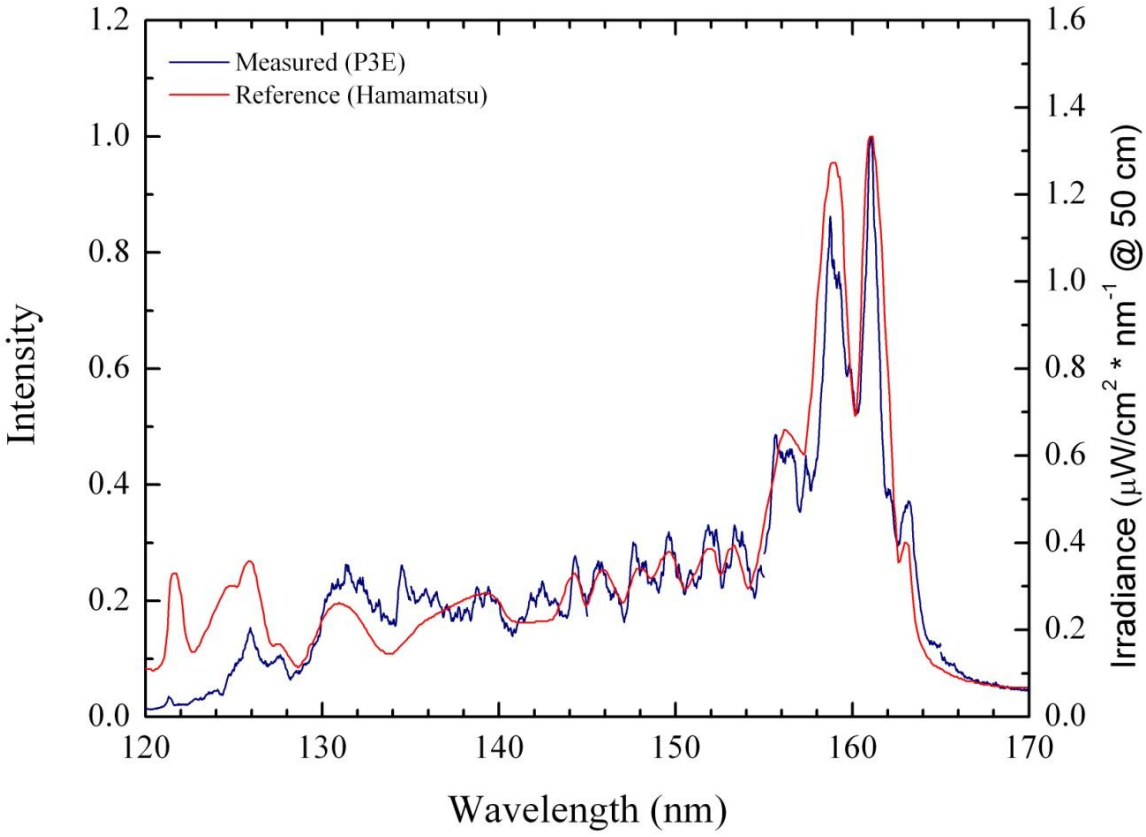

Figure 4.1: Comparison of measured response of the VUV lamp to manufacturer response [36].

The experimental profile is calculated from the ratio of the measured and supplied calibration curves. By dividing the two curves, a loss correction factor can be derived which will need to be multiplied with emission from flashover. The correction factor calculated from the measurement in Figure 4.1 is given in Figure 4.2. Note that the curve

is mostly flat above 140 nm, so the limited correction in this range makes building a temperature profile between 140 and 150 nm a somewhat more accurate process. Note that below 130 nm, the correction factor grows steeply corresponding to the correction required from the loss of VUV light in MgF_2 down to its cutoff wavelength of 115 nm.

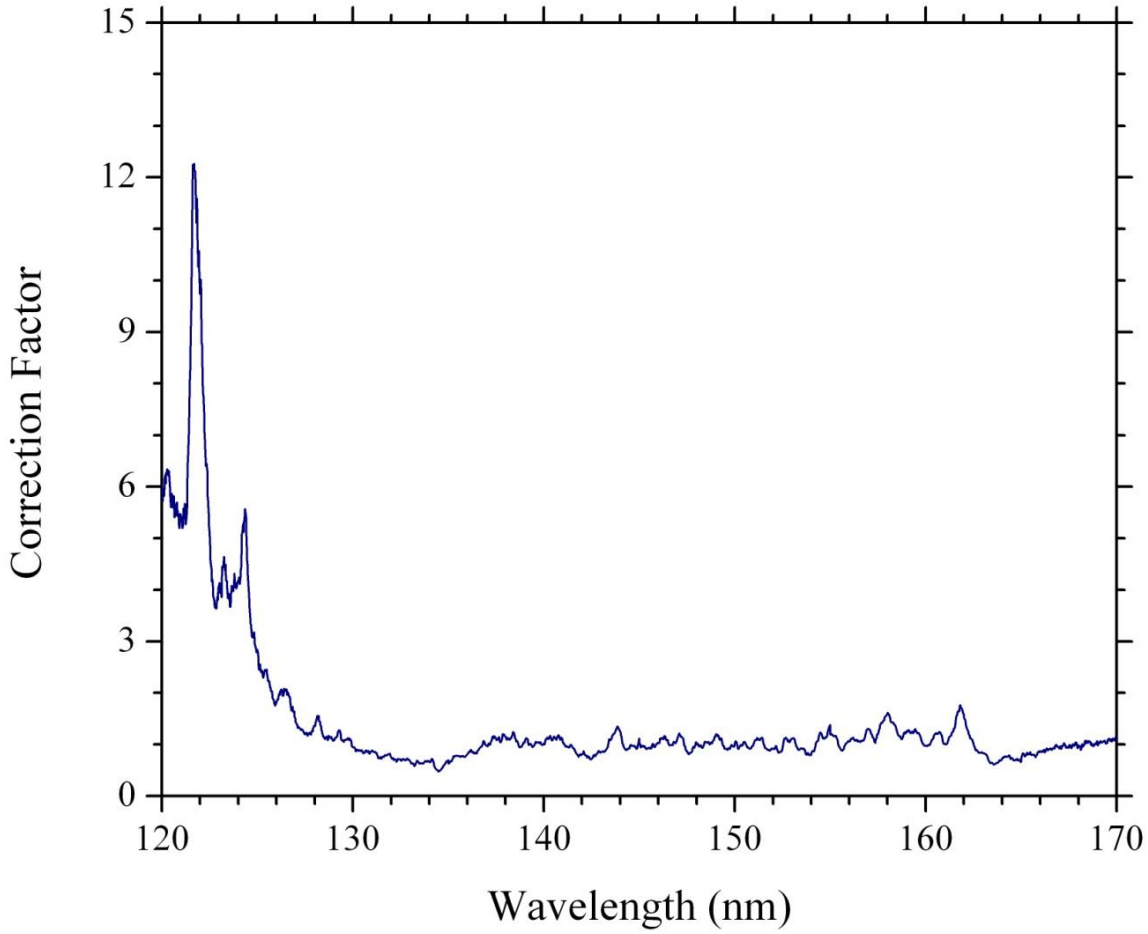

Figure 4.2: Correction factor which compensates for losses in the experimental apparatus.

4.1.2 Absorption as a Function of Distance

A possible concern is the liftoff of the flashover event from the window surface. Because of the loss of VUV light in atmospheric air, even a small liftoff could result in significant absorption and limited recorded intensity below 180 nm. As a test for this absorption, the broad spectrum VUV lamp was positioned at intervals from zero to 2 mm away from the entrance of the light path. The procedure was repeated from the last section for these distances, and the result of the measurement is recorded in Figure 4.3:

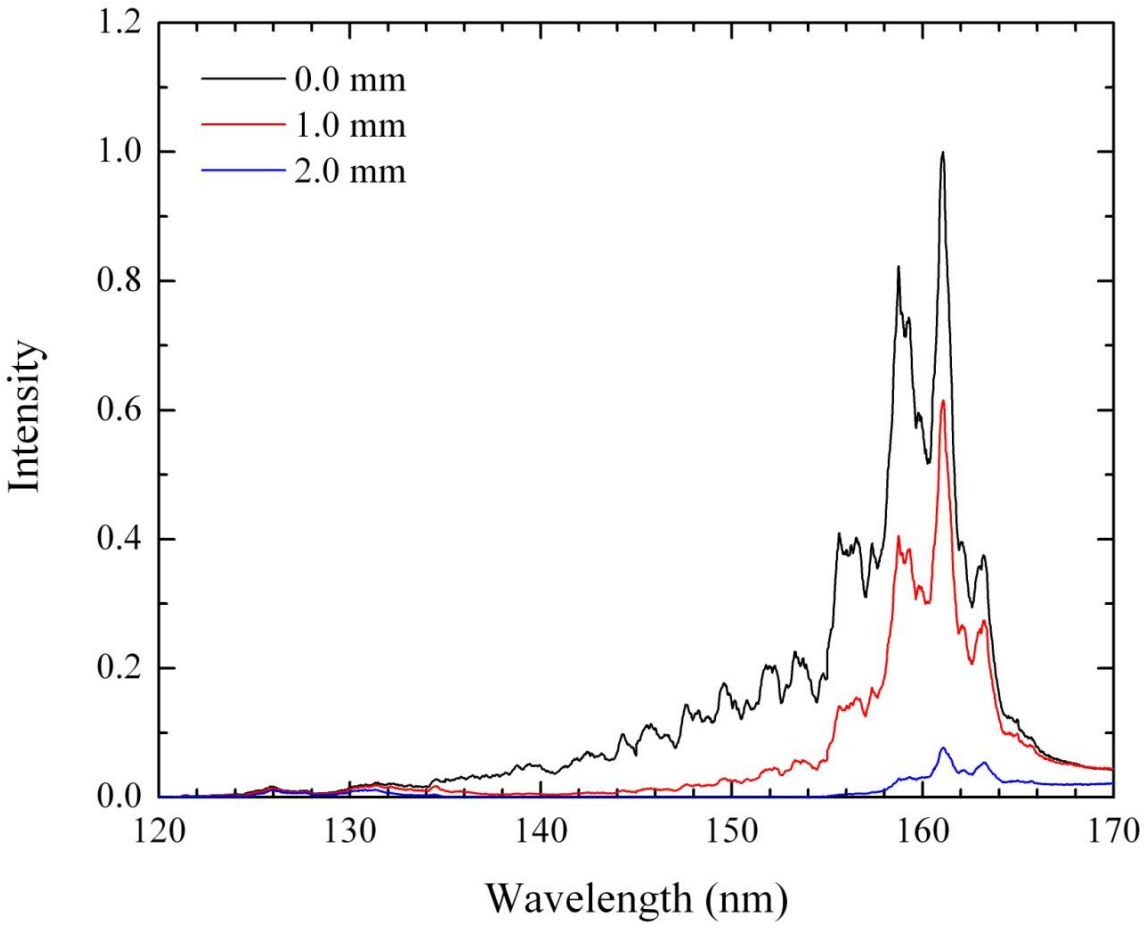

Figure 4.3: VUV absorption in air as a function of distance from the beamline entrance.

At first glance, the transmission of VUV below 180 nm decreases as a function of increasing air gap between the lamp and window surface. The peak intensity has been normalized in the case where the lamp is resting on the entrance surface, so a change of just 2 mm air gap results in 95% absorption of recorded emission between 135 and 180 nm. However if the range below 135 nm is selected, the zoomed area shows that the light is absorbed much less (see Figure 4.4):

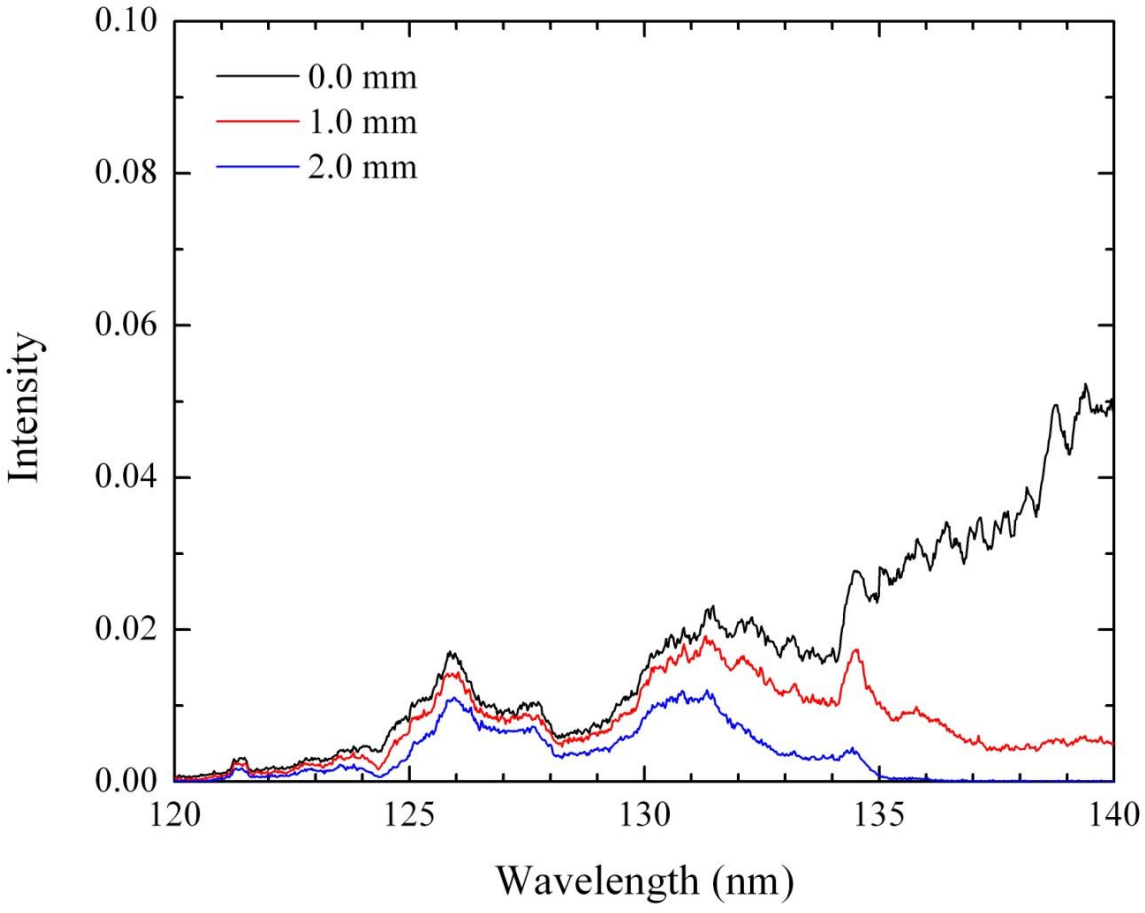

Figure 4.4: VUV absorption in air below 135 nm, as a function of air gap distance.

Note that while above 135 nm VUV light is essentially all absorbed in an air gap of 2 mm, easily 60% of emission below 135 nm still propagates through this air distance (see Figure 4.5, in agreement with Figure 2.5). This may be of significant consequence for streamer propagation, as photons must be able to propagate a number of millimeters before interacting with molecules in order to promote fast breakdown. Because the emission between 120 and 130 nm corresponds to excitation modes in atomic nitrogen and oxygen (shown in the next section), it is certainly of consequence that these photons are able to propagate longer distances in atmosphere.

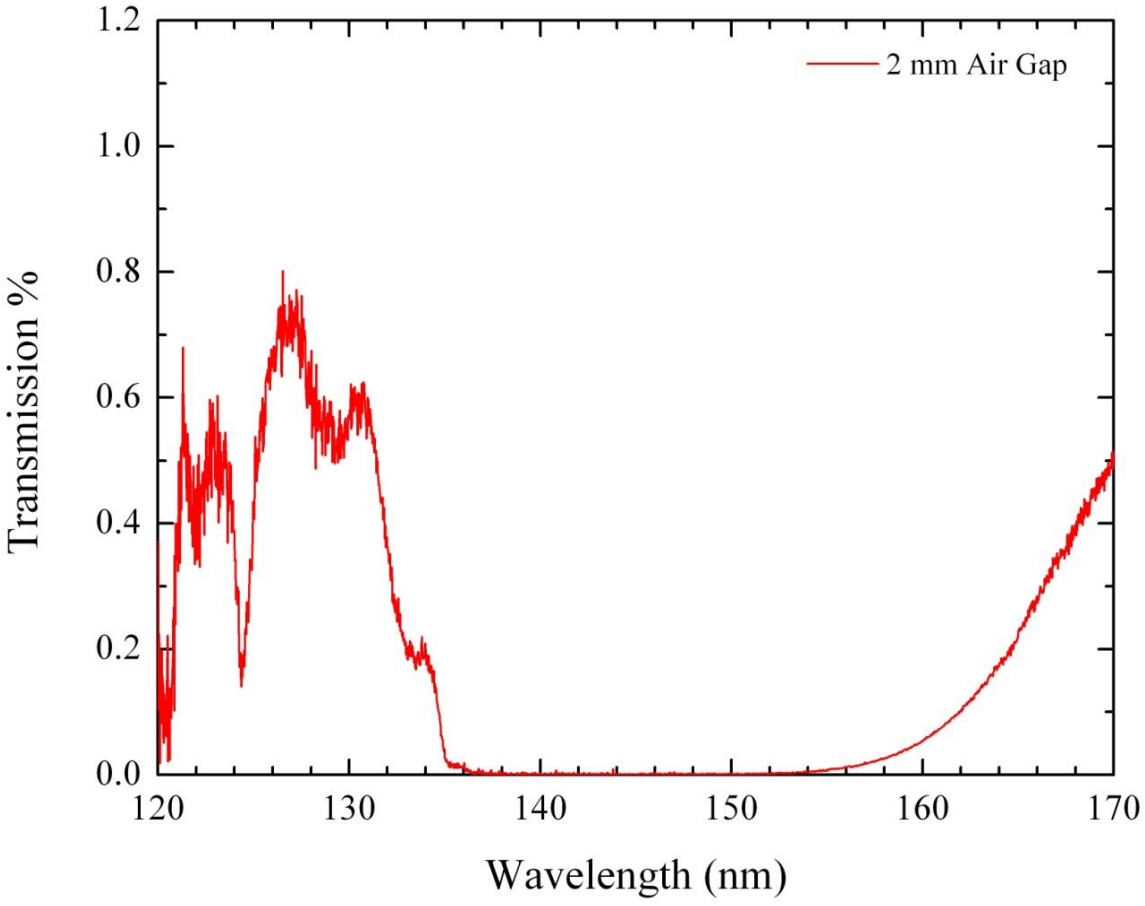

Figure 4.5: Measured transmission of VUV light through a 2 mm air gap.

4.2 VUV Emission from Breakdown

The primary objective of this project is to observe the vacuum ultraviolet emission from pulsed dielectric surface flashover events, with specific interest in the impact of VUV photons on streamer propagation. For this, the emission from atmospheric discharges is recorded and compared against simulated emission profiles. In addition, the emission characteristics are studied in gated intervals to determine the time periods of peak VUV emission.

4.2.1 Measured Emission

Utilizing the ICCD camera it was possible to integrate the VUV emission during the full duration of the flashover event (see Figure 4.6). For these measurements the camera was gated for 2 μs with high gain, with a light flow of dry air into the flashover chamber for roughly 30 seconds before voltage triggering. Five flashover events are accumulated at 20 nm intervals between 100 and 200 nm. As indicated, virtually all prominent emission lines are identified as being emitted from atomic oxygen and nitrogen between 120 and 180 nm. The intensity of the measured VUV emission drops rapidly below 135 nm, which is attributed primarily to the falling transmission of MgF_2 down to its cutoff wavelength of 115 nm. The exact emission lines which could be easily identified from the surface flashover event have been tabulated in Table 4.1, with Einstein coefficients, degeneracies, and electron configurations from NIST [15].

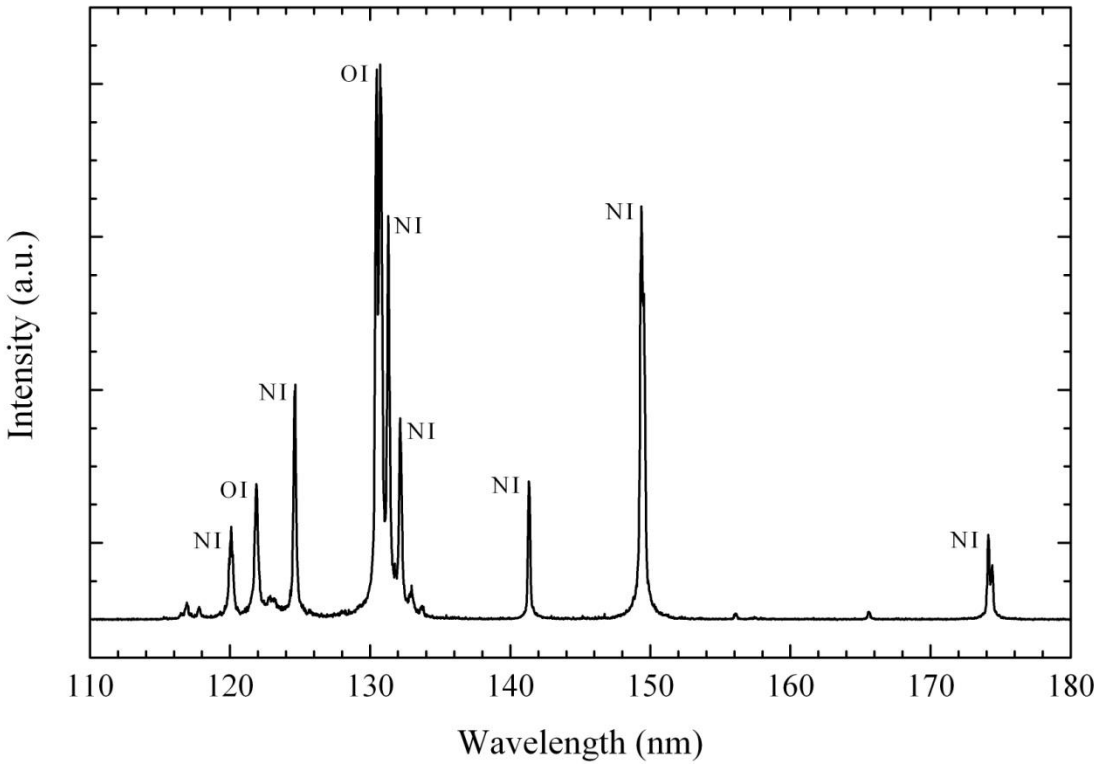

Figure 4.6: Recorded VUV emission from an atmospheric discharge in air.

Table 4.1: Vacuum UV emission lines from atomic nitrogen and oxygen which can be identified from surface flashover in atmosphere ($^{\psi}$ ground transitions).

Species	Wavelength [nm]	A [s^{-1}]	Energy [eV]	Configuration	g_i - g_k
NI$^{\psi}$	120.02	3.99×10^{8}	10.33	$2s^22p^3$ - $2s^22p^2(^3P)3s$	4 - 4
OI	121.76	2.06×10^{8}	10.18	$2s^22p^4$ - $2s^22p^3(^2P°)3s$	1 - 3
NI	124.32	3.21×10^{8}	9.97	$2s^22p^3$ - $2s^22p^2(^1D)3s$	6 - 6
OI$^{\psi}$	130.22	3.41×10^{8}	9.52	$2s^22p^4$ - $2s^22p^3(^4S°)3s$	5 - 3
OI	130.49	2.03×10^{8}	9.50	$2s^22p^4$ - $2s^22p^3(^4S°)3s$	3 - 3
NI	131.05	8.42×10^{7}	9.46	$2s^22p^3$ - $2s^22p^2(^3P)3d$	4 - 6
NI	131.97	6.33×10^{7}	9.40	$2s^22p^3$ - $2s^22p^2(^3P)3d$	4 - 4
NI	141.19	9.59×10^{6}	8.78	$2s^22p^3$ - $2s^22p^2(^1D)3s$	4 - 4
NI	149.26	3.13×10^{8}	8.31	$2s^22p^3$ - $2s^22p^2(^3P)3s$	6 - 4
NI	149.47	3.72×10^{8}	8.30	$2s^22p^3$ - $2s^22p^2(^3P)3s$	4 - 2
NI	174.27	1.16×10^{8}	7.12	$2s^22p^3$ - $2s^22p^2(^3P)3s$	4 - 4
NI	174.53	9.22×10^{7}	7.10	$2s^22p^3$ - $2s^22p^2(^3P)3s$	2 - 2

As a double check for the identification of the emission lines below 135 nm, the ICCD recording procedure was repeated for atmospheric pressure discharges in a nitrogen environment. For these measurements, high purity dry nitrogen (less than 1 ppm impurity) was used in light flow. Note that while high purity gas was used, there is no guarantee that the flashover chamber is 100% completely filled with nitrogen, and small trace amounts of other atmospheric gases may still be present even after minutes of light flow. The result of the measurements below 135 nm in both dry air and high purity nitrogen are given in Figure 4.7:

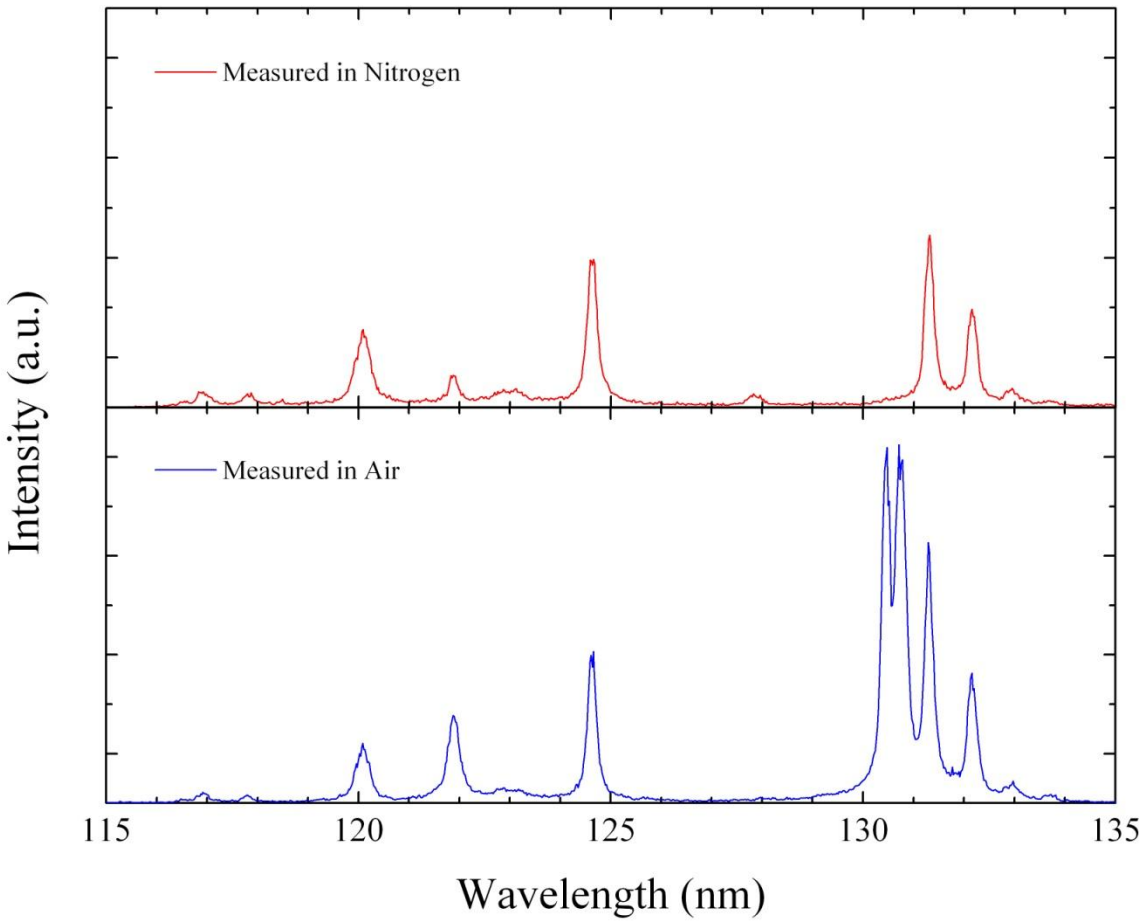

Figure 4.7: Comparison of VUV emission from dry air and nitrogen discharges.

Note that the emission in both high purity nitrogen and dry air are largely similar in this range. Oxygen emission lines at 121.8, 130.2, and 130.6 nm are highly suppressed in the pure nitrogen environment, as compared to air. The recorded nitrogen emission intensity changes very little between the two gases, except for the magnitude of the nitrogen lines at 131.0 and 131.9 nm. However, the Lorentz line width profile is fairly large in our setup (discussed in the next section), and so it is estimated that the removal of the intense oxygen lines at 130.2 and 130.6 nm can result in the lower intensity nitrogen peaks at 131.0 and 131.9 nm.

4.2.2 Simulated Emission

The primary identification mechanism for emission lines is through the simulation of probable atomic and molecular transitions in a gas. The simulation package used in this study is SpectraPlot, a temperature dependent spectral software suite developed by Dr. Andreas Neuber at Texas Tech University. This software uses the National Institute of Standards and Technology (NIST) Atomic Spectra Database [15], which is an exhaustive list of atomic transitions, Einstein coefficients, and probabilities. SpectraPlot assumes a Boltzmann distributed electronic population density, and utilizes user defined Lorentz, Gaussian, and rectangular line width profiles to calculate the atomic emission lines. By varying the input temperature of the simulation, the line ratios can be calculated to match the ratios observed in measurement to estimate the temperature in the discharge.

As discussed previously, the apparatus profile is fairly flat in the region between 140 and 150 nm, so this region would require the least (or no) correction for absorption. Thus the easiest emission lines for calibration of temperature would be the isolated nitrogen lines between 141.2 and 149.5 nm. For this process, the emission line at 141.2 nm is normalized in both simulation and measurement, while the simulation is altered until the line profile of the 149.5 nm peak agrees with measurement. It can be shown that the most accurate line profile results from an estimated Boltzmann temperature of 10 ± 4 eV (see Figure 4.8). For this profile, the line widths are estimated as Lorentz = 0.17 nm, Gauss = 0.02 nm, and rectangular (slit) = 0.05 nm. Note that the experiment cannot completely resolve the double nitrogen peak between 149.3 and 149.5 nm, and as a result the measurement exhibits some uncertainty at the maximum at 149.3 nm when compared to the simulation. However as a whole, the line simulation seems to match the observed line width for the rest of the profile. The estimated error (discussed in Appendix B) is somewhat significant for this measurement as a result of using only two emission lines for the calculation, the slight uncertainty in shot-to-shot intensity jitter, and to sensitivity to the accuracy of the NIST tabulated Einstein coefficients which for these lines can vary as much as 25%.

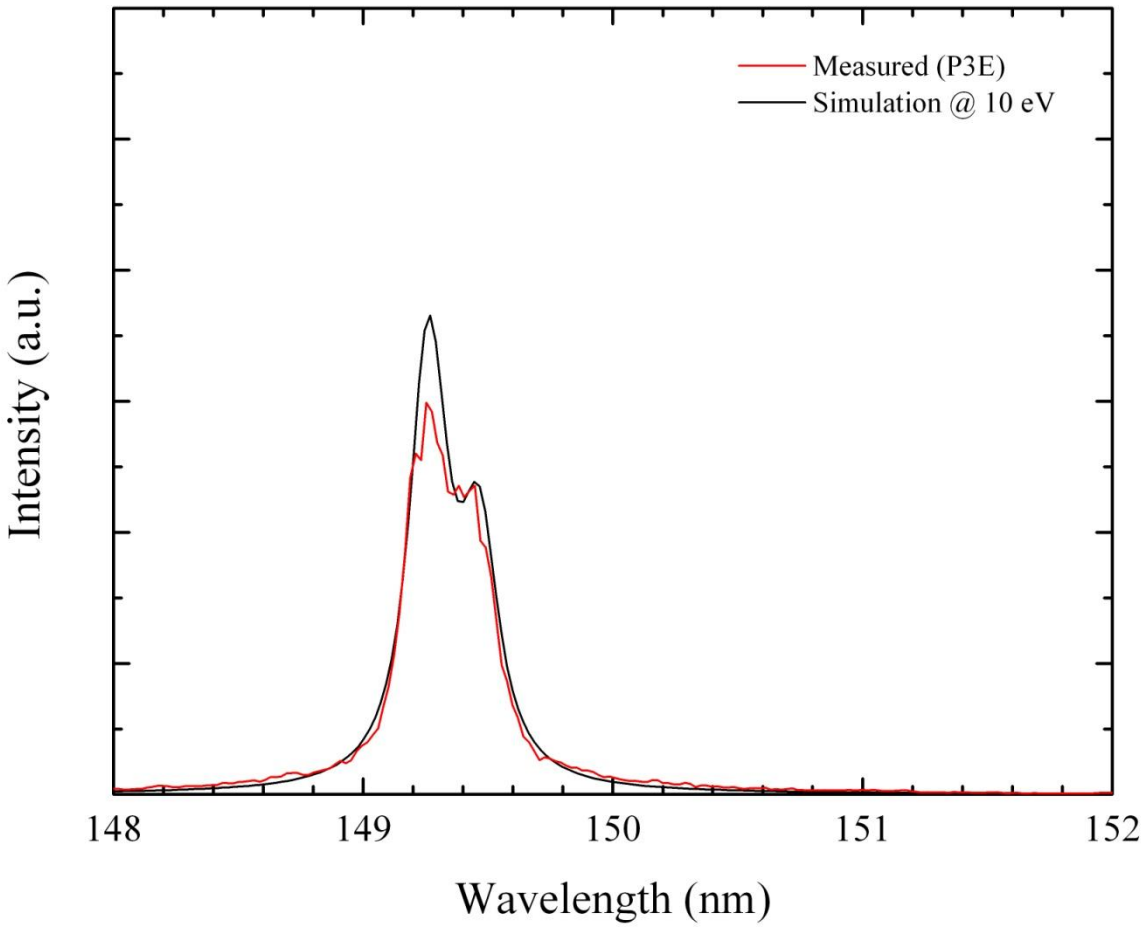

Figure 4.8: Comparison of measured and simulated nitrogen double emission line at 149.5 nm used for temperature estimation.

Using this simulated temperature estimate at 10 eV, the complete VUV emission spectrum can be calculated (see Figure 4.9). Note that the majority of the line structure from simulation matches the observed emission from experiment. The measured line decay below 135 nm is due to absorption of MgF_2 in the optical materials. In addition, the oxygen line at 130.2 corresponds to a ground transition, so it would seem that this line could be strongly self-absorbed as compared to the simulated 10 eV emission line. This self-absorption agrees with the lack of intensity of this 130.2 nm line compared to the

similar 130.5 nm oxygen line in simulation. Most importantly, virtually all lines between 120 and 180 nm can be identified as an atomic excitation from nitrogen or oxygen, which would imply that a mechanism exists which dissociates atmospheric gases during breakdown.

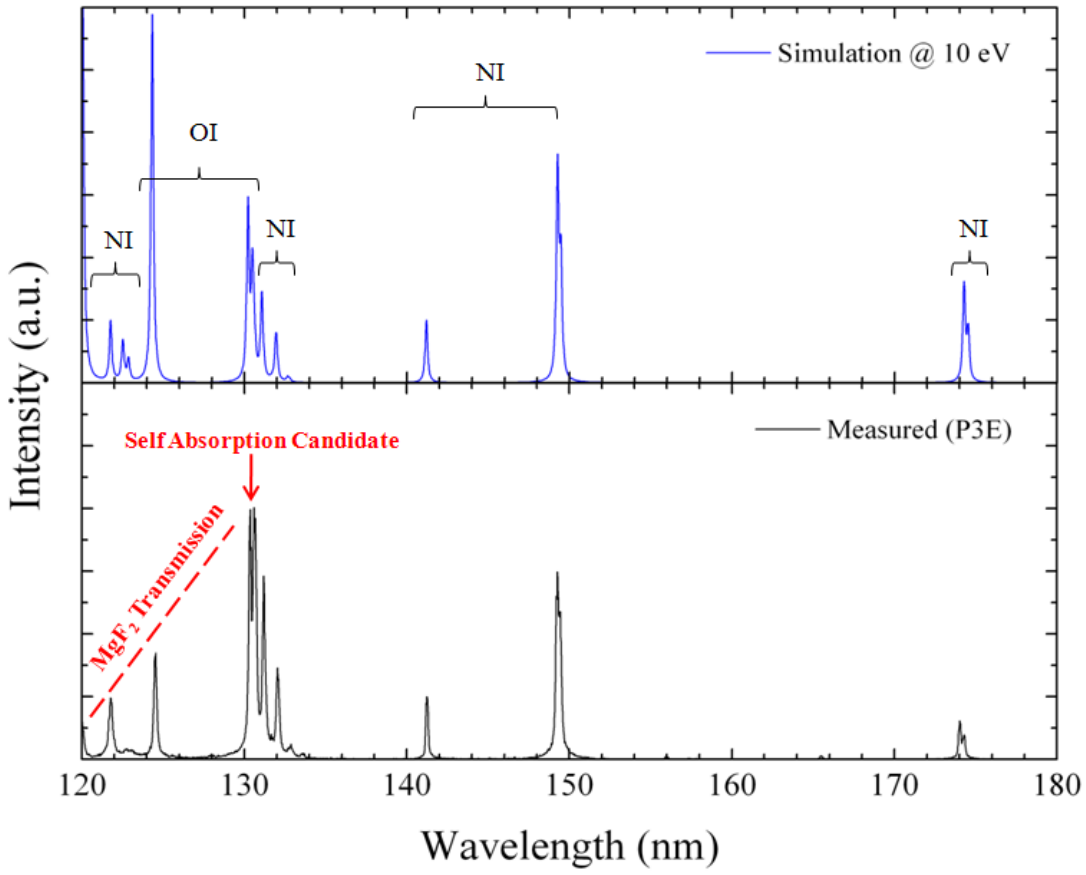

Figure 4.9: Comparison of measured VUV emission from surface flashover and 10 eV spectral simulation.

4.2.3 Timed Resolved Spectroscopy

It should be noted that the most significant VUV activity in pulsed atmospheric discharges is observed during the initial fast stage of streamer propagation. This was confirmed by measuring the intensity of an atomic nitrogen emission line at 141.2 nm for gated 100 ns intervals during the discharge period (using the ICCD, see Figure 4.10). Maximum VUV emission occurs during the initial stage of discharge (also confirmed by PMT measurements, see Figure 4.11).

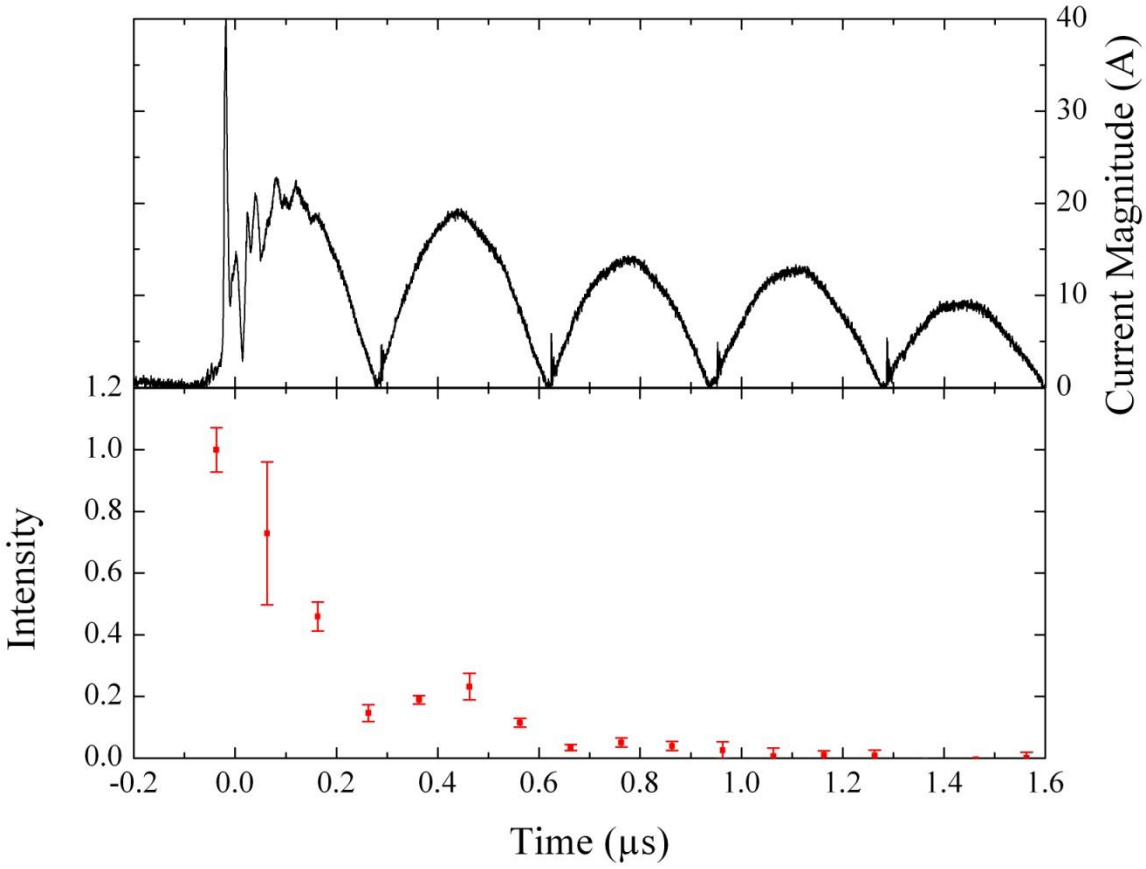

Figure 4.10: Timed spectroscopy of the 141.2 nm line, compared to current magnitude during breakdown.

Emission of VUV rapidly declines after full conduction occurs, with small resurgence at 200 and 600 ns. This resurgence is caused by the undamped current in the flashover circuit switching polarity with a half wave period of around 400 ns. This can be qualitatively understood as being caused from the discharge plasma heating and cooling during current zero crossings, where small VUV re-emissions could occur. However, there is obviously very limited VUV production for the remaining microseconds of the discharge where the current is still high, but the voltage has collapsed.

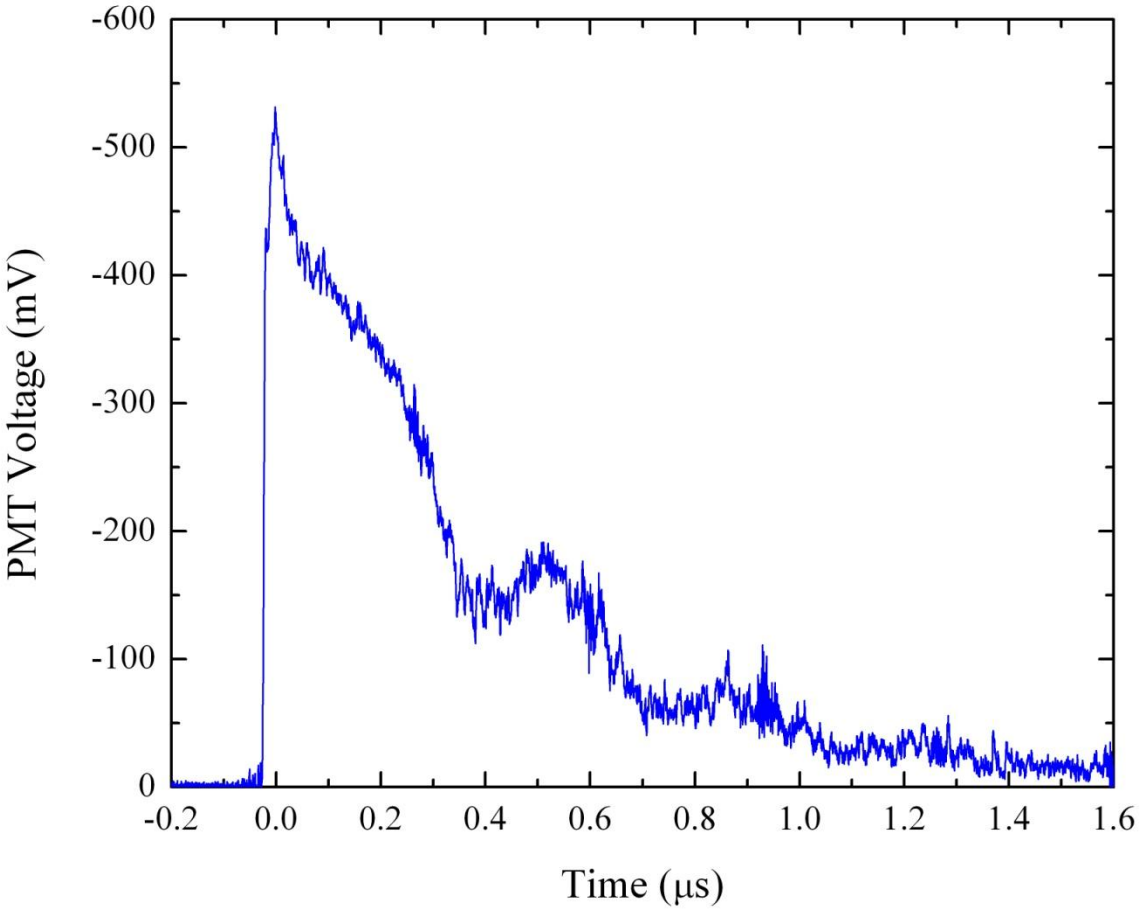

Figure 4.11: Recorded PMT signal corresponding to the decay of the 141.2 nm nitrogen emission line.

The timed ICCD gated procedure discussed was repeated for a number of excitation lines between 130 and 150 nm (see Figure 4.12). The error bars have been removed for clarity, but the standard deviation is similar to the measurement used in Figure 4.10. All emission lines have been normalized at the same peak intensity so as to make a decay comparison.

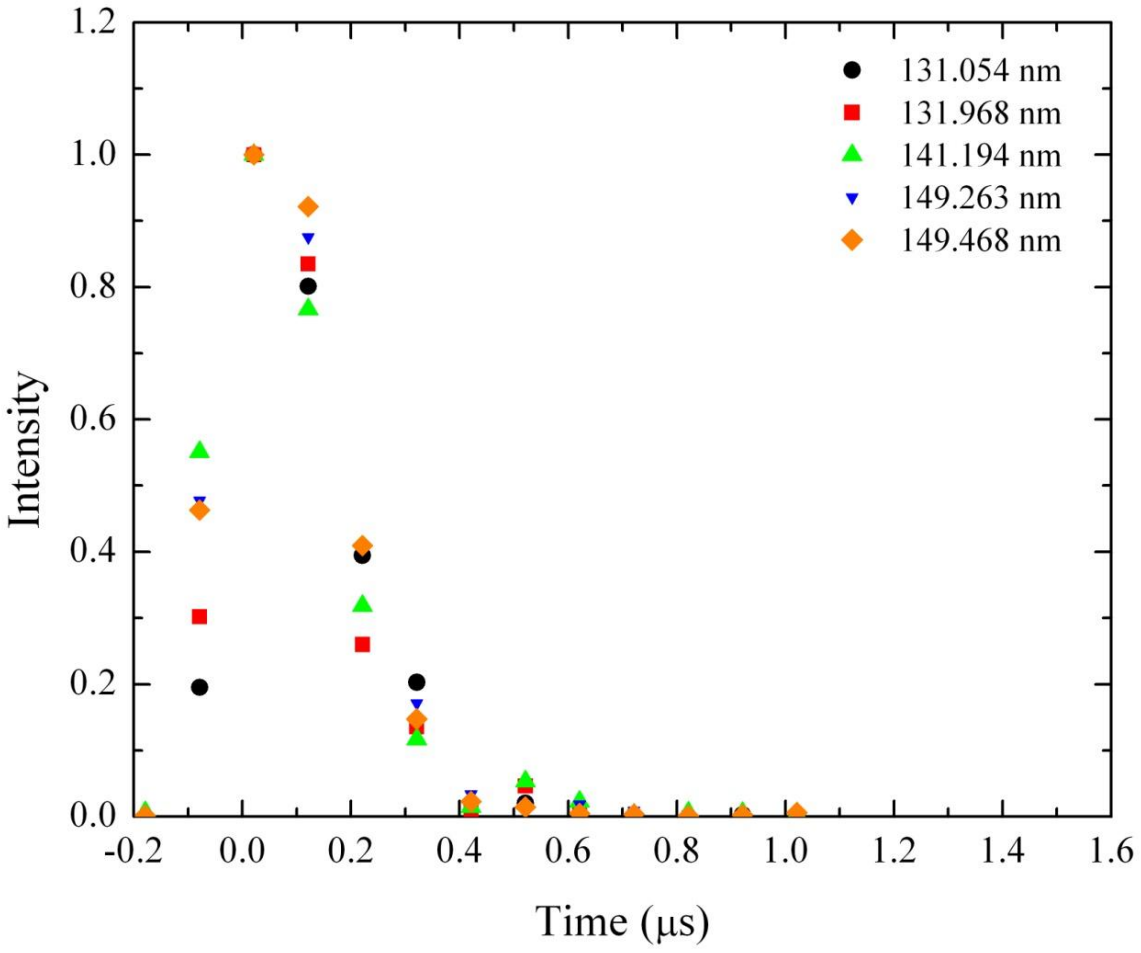

Figure 4.12: Timed ICCD gated spectroscopy for multiple emission lines during atmospheric discharges.

While the insertion rates may be slightly different between lines, qualitatively there does not seem to be any significant deviation in decay rates of the emission lines after peak intensity. All VUV activity is observed during the fast breakdown phase and for the first few hundred nanoseconds, with limited VUV production for the remaining microseconds of the discharge. Note that the current waveform was more damped (higher circuit resistance) in this measurement than what was present for the measurement in Figure 4.10, so the resurgence of VUV after the first half wave seems to have also been damped in comparison.

The timed spectral study can be used to estimate the number of atoms that radiate in the plasma, which gives an order of magnitude estimate to the number of dissociations which much occur during the initial stage of breakdown. The detailed math is shown in Appendix B, but the essential results have been tabulated below. Note that the only lines used in this estimation were the two nitrogen lines used also in the temperature simulation. The partition function for nitrogen (Z = 450.71 from NIST [15]), the gate time (100 ns), essential geometric parameters from the optical light path, and temperature (T = 10 eV) are assumed:

Table 4.2: Emission parameters used to estimate the number of radiating atoms in the plasma during the fast breakdown stage (see Appendix B for details).

Parameter	Value (Line 1)	Values (Line 2 - Composite)		
Wavelength (nm)	141.1939	149.2625	149.2820	149.4675
ICCD Counts	1085		5088	
Quantum Efficiency @ λ	13.2%		13.2%	
MgF2 Transmission @ λ	37.0%		44.1%	
Mirror Reflectivity @ λ	81.0%		79.0%	
Corrected Emission @ λ	2.05×10^{6}		6.12×10^{6}	
Wavenumber (cm^{-1})	99663.912	86220.51	86220.51	86137.35
Energy Level Degeneracy	4	4	4	2
Einstein Coefficient (s^{-1})	9.59×10^{6}	3.13×10^{8}	3.51×10^{7}	3.72×10^{8}
Parent Energy Level (eV)	12.36	10.69	10.69	10.68
Population of Level	3.33×10^{6}		1.86×10^{7}	
Estimated No. of Atoms	**1.29×10^{9}**		**2.44×10^{9}**	

This order of magnitude approximation seems to be in agreement for the two nitrogen lines in this range, and gives an estimated number of atoms around 10^{9}. If we assume a plasma volume on the order of 1 mm^{3}, then the density of atoms (which could be a reasonably similar density as the number of molecular dissociations) is on the order of $10^{12}/cm^{3}$. Because atmospheric pressure gases have a density on the order $10^{19}/cm^{3}$, then roughly one molecule per ten million must be dissociated during the fast stage of breakdown.

4.3 Breakdown Waveforms

Using the electrical diagnostics it was possible to achieve nanosecond scale recording of both voltage and current during the fast phase before voltage collapse. Typical voltage and current waveforms recorded during a flashover event in air are shown in Figure 4.13. The voltage rises across the flashover electrodes until roughly 25 ns before breakdown, when voltage fluctuations set in and the current begins to slowly rise. Note that the voltage fluctuations are mirrored by current fluctuations, as one would expect that the gap voltage reduces when the gap current increases. The small peaks at -17 and -14 ns could be due to small electron avalanches that are not energetic enough to fully connect the electrode gap, but are large enough to be recorded by the current diagnostics. Integration of these small current peaks reveals an estimated electron number of 1.21×10^9 and 2.43×10^9 electrons. The peak current amplitude and duration is limited by the external circuit with an effective gap capacitance, C_p, estimated to be on the order of 10 pF. This fast current stage is followed by a slow phase at intermediate current amplitude where the driving voltage, see Figure 3.5, slowly pushes current through the gap limited by the somewhat large parasitic inductance, L_p, of the wire leads between gap and the pulse transformer. The duration of this current pulse is a few microseconds (as shown in Figure 4.10) and is intentionally cut off in Figure 4.13 as it is irrelevant for the study of the mechanisms leading to breakdown. The half wave period for the current oscillations is around ~200 ns, and this period qualitatively agrees with the small resurgence of VUV intensity of similar period, as discussed in the previous section (see Figure 4.10).

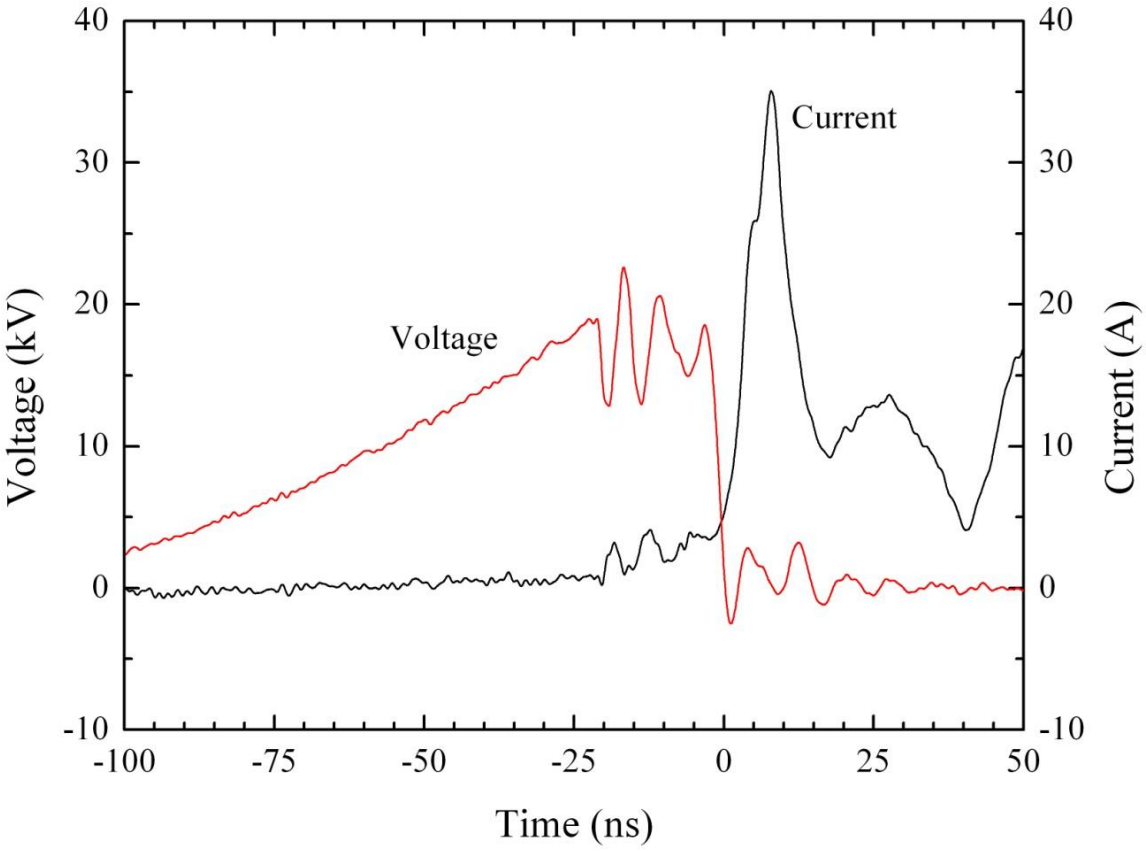

Figure 4.13**:** Typical voltage and current waveforms during a flashover event.

This period before full breakdown corresponds to the fast streamer phase, where photoionization is believed to play a major role. This is consistent with the observed VUV emission activity measured by the PMT during this same streamer period (see Figure 4.14). The PMT intensity observed for 149.5 nm (which corresponds to atomic nitrogen emission double peak) rapidly increases in the few nanoseconds before full spark breakdown, followed by a falling voltage and rising current to peak values. The oscillating activity of recorded VUV intensity which begins from -60 ns before breakdown could be caused by small noise in the diagnostics, but the general trend is that

the oscillations have a negative net slope indicating VUV emission during this period before voltage collapse. This would agree with the streamer theory which states that energetic photons play a primary contributing role in the development of fast avalanches which lead to spark breakdown. The peak VUV intensity is observed around -5 ns before full voltage collapse, which indicates that a massive amount of photoionization could be driving the current rise at breakdown.

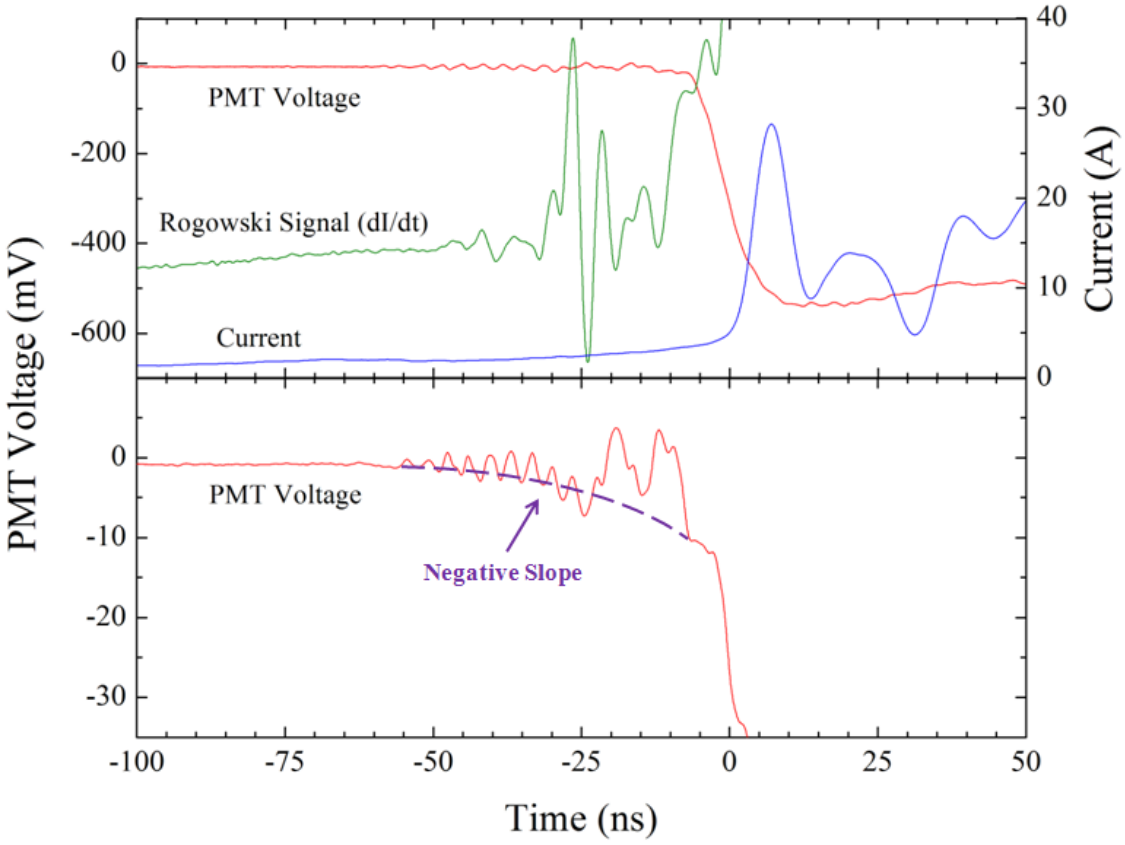

Figure 4.14: Typical recorded 16-shot average PMT intensity and current (small and large zoomed scale) for the 149.5 nm emission line during breakdown.

4.4 Flashover Imaging

It was also desired to image the development of flashover with an ICCD camera on the atmospheric side, with a time resolution on the order of nanoseconds. Images were taken of fast breakdown events in pure nitrogen, pure oxygen, and dry air environments at atmospheric pressure. The ICCD gate information coupled with fast electrical diagnostics allows for exact reconstruction of the event timing for observed images recorded during the streamer phase precluding voltage breakdown.

4.4.1 Nitrogen Streamers

Images were taken of triggered surface flashover events in a pure nitrogen environment (less than 1 ppm impurity). For this procedure the atmosphere ICCD camera was gated for 3 ns and the voltage diagnostic compared with the ICCD gate diagnostic allowed for the reconstruction of image timing with respect to the instant of voltage collapse. The result of this measurement is given in Figure 4.15 (all times shown are measured from the moment of full voltage collapse). As indicated, the top left electrode is the anode and the bottom right electrode is the cathode, which are floating connections to the secondary of the pulse transformer. In the time up to 60 ns before breakdown the electrodes become very luminous, where the high field region accelerates electrons and leads to collisional excitations causing early photon emission. These photons travel away from the anode and can cause excitations and ionizations of the gas molecules in the gap, where the regions of highest activity are coupled with luminous

streamer heads. This is confirmed by some initial activity of streamers showing they propagate away from the top anode towards the bottom cathode during the time before 40 ns. These streamers are also attracted to the outside steel flange which houses the MgF_2 window surface.

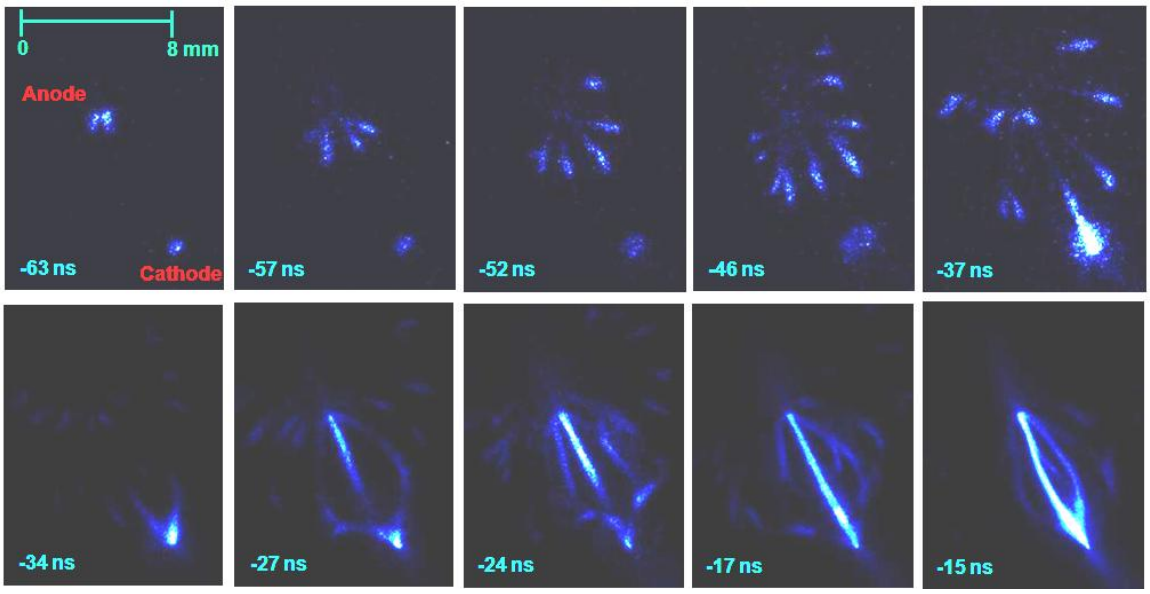

Figure 4.15: Imaging of surface flashover in nitrogen environment at atmospheric pressure, with recorded gate times of 3 ns.

The estimated propagation velocity of these early streamers is around $4x10^7$ cm/s, which is on the order of what other groups have observed [4-5]. Around 40 ns before breakdown the streamers (corresponding to VUV photon driven ionization) connect with the cathode and secondary processes begin to fill the gap. At this point the recorded PMT intensity begins to decay with a negative slope indicating VUV emission during this period (see again Figure 4.14). The electrons which were initially produced from volume photoionization and possibly photoemission from the surface during the early

stage have now already channeled away, and only positive ion space charge remains. It appears that the first series of cathode directed streamers (all recorded events originate from the anode) are insufficient to produce a fully conducting channel (see the connected streamers at t = -37 ns). While the pulse voltage is still increasing at ~200 V/ns, second generation cathode directed streamers cause the visible fluctuation in the current waveform at early times (see again Figure 4.13). Eventually a fully conducting channel is established and main current starts to flow with a comparably sharp rise time. The only energy available for this sharp current rise is stored in the parasitic capacitance of the setup, C_p, estimated to be of the order of 10 pF, charged to the flashover voltage. More current starts flowing after the initial current spike due to the main 25 nF capacitor pushing current through the pulse transformer and discharging through the flashover gap. The basic shape of the breakdown channel remains unchanged for times larger than -15 ns, and the intensity of the spark's self luminosity is increasing significantly.

4.4.2 Oxygen Streamers

While the nitrogen streamers are very self contained during the 3 ns ICCD gate intervals (meaning that limited emission occurs in the wake of a streamer head before -37 ns in Figure 4.15), the same cannot be said of images observed in a pure oxygen environment (see Figure 4.16). During the times before -43 ns before voltage collapse, a diffuse amount of oxygen emission activity is observed even in the wake of passing streamer heads. This is clear at -38 ns, where even after the streamer heads have

connected the electrode gap distance, diffuse emission is still observed in the entire gap during the 3 ns of the gated image. The first streamer heads which propagate the gap are unsuccessful in creating a fully conducting channel, as in the pure nitrogen case. However a volume process seems to begin after -31 ns before voltage collapse, until -14 ns when a strong anode directed streamer is emitted from the cathode region and fully connects the gap by -7 ns before breakdown. This is in contrast to the strong anode directed streamer from the nitrogen case.

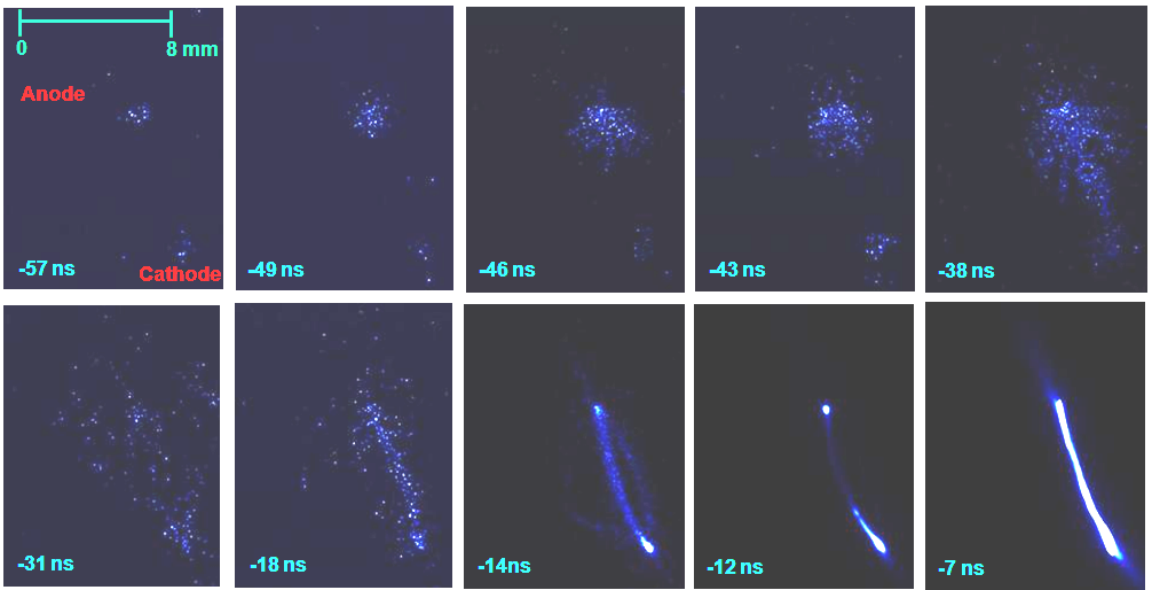

Figure 4.16: Imaging of surface flashover in oxygen environment at atmospheric pressure, with recorded gate times of 3 ns.

4.4.3 Air Streamers

The final imaging set was taken in a dry air environment at atmospheric pressure (see Figure 4.17). While nitrogen streamers were very segmented and oxygen streamers were very diffuse, the air streamers exhibit a combination of diffuse and segmented behavior. In the time up to -38 ns before breakdown, the streamer heads are clearly attracted both to the cathode and the grounded flange around the window, but the wake of these streamers are showing continuous emission behavior as in the pure oxygen case. Because both nitrogen and oxygen discharges produce failed initial attempts of full conduction, it is no surprise that the air discharge also fails to breakdown after the first stage of connecting streamers. However of interest is the combination of anode directed and cathode directed activity in the period up to -14 ns, which culminates in the space charge attracted streamers connecting in the middle of the gap at breakdown.

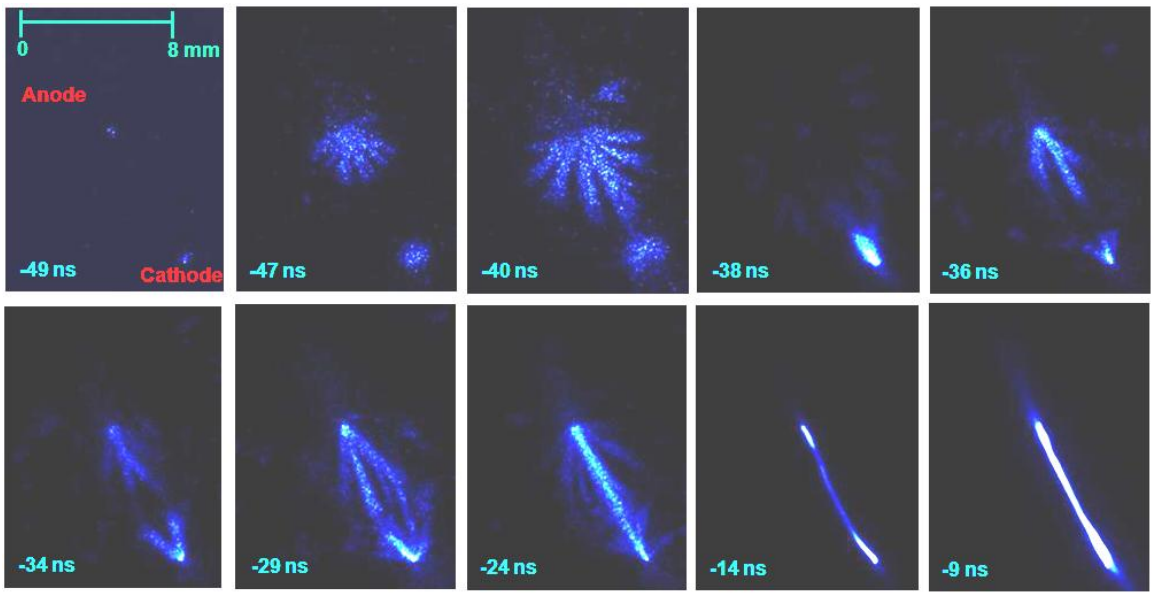

Figure 4.17: Imaging of surface flashover in dry air environment at atmospheric pressure, with recorded gate times of 3 ns.

4.5 Field Simulation

An electrostatic field model was constructed to simulate the conditions before voltage collapse, using the Ansoft Maxwell® software package. This model assumes an electrode tip radius of 200 μm, and is simulated for an applied voltage of 20 kV with three different electric field geometries. The applied voltage was chosen because it was shown that breakdown occurs are roughly 22 kV and it was desired to simulate the field enhancement factor at the triple point between electrode, dielectric surface, and atmosphere. A corresponding set of streamer images were recorded by the ICCD, and accompany the different electric field geometries. A number of significant observations can be drawn for each situation, and the streamer process clearly varies as a function of the applied field.

4.5.1 Symmetric Field Geometry

The primary field configuration used in this study was designated "symmetric" because the transformer secondary is applied directly to the electrodes on the flashover gap. While the steel flange housing the window remains "hard" grounded to the structure, the cathode is understood to be at a negative high voltage while the anode is at positive high voltage, with the total potential difference equal to 20 kV. As such, the cathode in simulation is excited to -10 kV and the anode to +10 kV, while the flange is grounded at 0 Volts. The resulting field simulation is shown in Figure 4.18 (magnitude only):

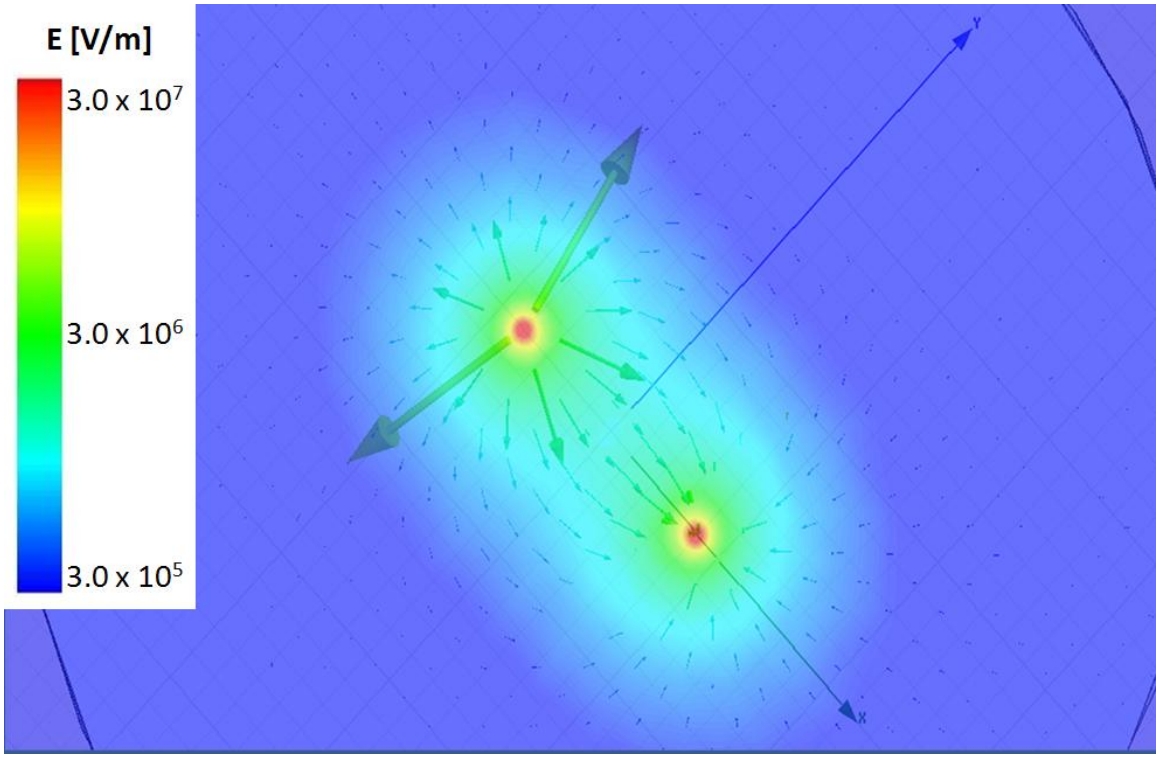

Figure 4.18: Simulation of electric field magnitude with symmetric electric field geometry.

As expected, the majority of the field vectors point from anode to cathode, with some pointing from anode to the outside steel housing. The large arrows in Figure 4.18 coming out of the anode are a software artifact, and are a result of the large field enhancement at the triple point. The ICCD imaging of streamers observed in the symmetric field excitation case are shown below in Figure 4.19, gate time 10 ns:

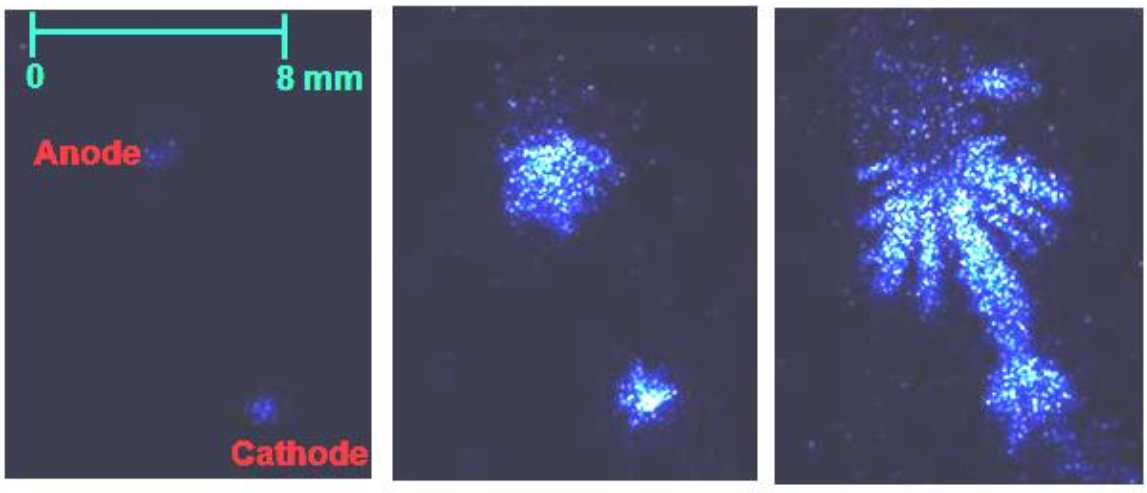

Figure 4.19: Streamer sequence observed under symmetric field excitation in air.

The essential streamer physics have been discussed in the previous sections, and as expected the streamers propagate from anode to cathode. The most luminous areas are in the vicinity of the high field region where the electrons are accelerated, and collisions emit VUV photons into the gap. While a majority of the streamers propagate in the direction of the greatest potential difference (i.e. the cathode), some propagate towards the outside flange which is at a potential between the anode and cathode.

4.5.2 Hard Grounded Geometry

If the cathode is directly attached to the steel housing structure of the flange, the resulting field geometry is designated “hard” grounded. Because the potential difference on the transformer secondary must remain 20 kV, the anode is considered to be at positive potential if the cathode is hard grounded to 0 Volts. Thus in simulation the

anode is excited to +20 kV while both the cathode and steel flange are grounded to 0 Volts. The resulting field simulation is shown in Figure 4.20 (magnitude only):

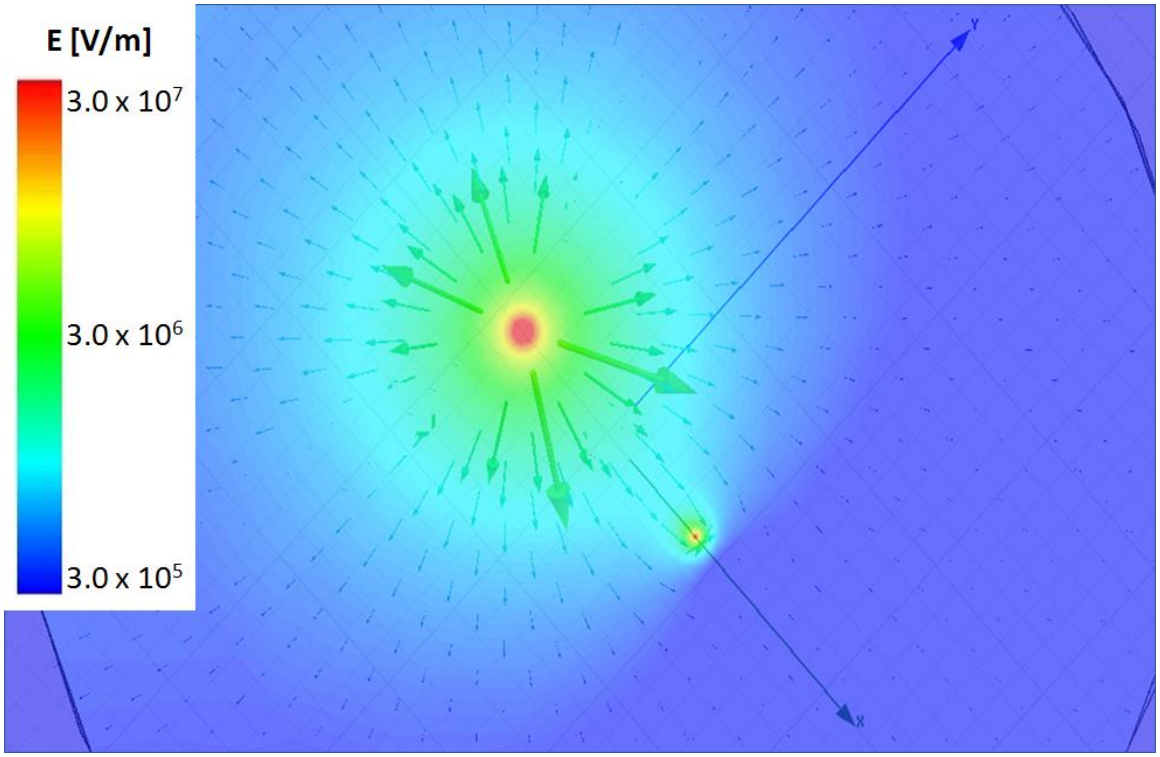

Figure 4.20: Simulation of electric field magnitude with the cathode hard grounded.

In this model the electric field vectors are equally pointing to both the outside steel flange and the cathode. The magnitude of the electric field near the anode is much larger than the field near the cathode, so the field enhancement factor is greatest in the vicinity of the anode. The ICCD imaging of streamers observed when the cathode is hard grounded are shown below in Figure 4.21, gate time 10 ns:

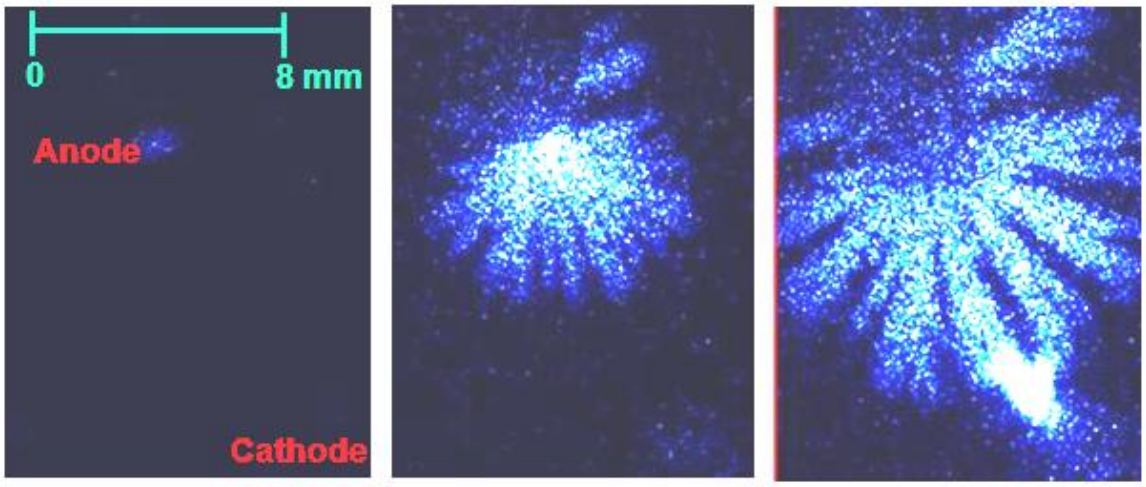

Figure 4.21: Streamer sequence observed when the cathode is hard grounded, in air.

The basic structure is similar to that of the symmetric field case, but now there are many more streamers forming in the region leaving the anode. This is mainly due to the fact that the field enhancement factor in the region surrounding the anode is much larger than in the previous case, so the electrons are accelerated in a stronger gradient and emit more VUV photons. Also note that the cathode shows much lower luminosity than in the symmetric field case, mainly because the field enhancement factor in this region is so low than almost no electrons are accelerated to the level where significant photon emission can take place.

4.5.3 Negative High Voltage Geometry

If the anode is directly attached to the steel housing structure of the flange, the resulting field geometry is designated as “negative high voltage.” Because the potential

difference on the transformer secondary must remain 20 kV, the cathode is considered to be at negative potential if the anode is hard grounded to 0 Volts. Thus in simulation the cathode is excited to -20 kV while both the anode and steel flange are grounded to 0 Volts. The resulting field simulation is shown in Figure 4.22 (magnitude only):

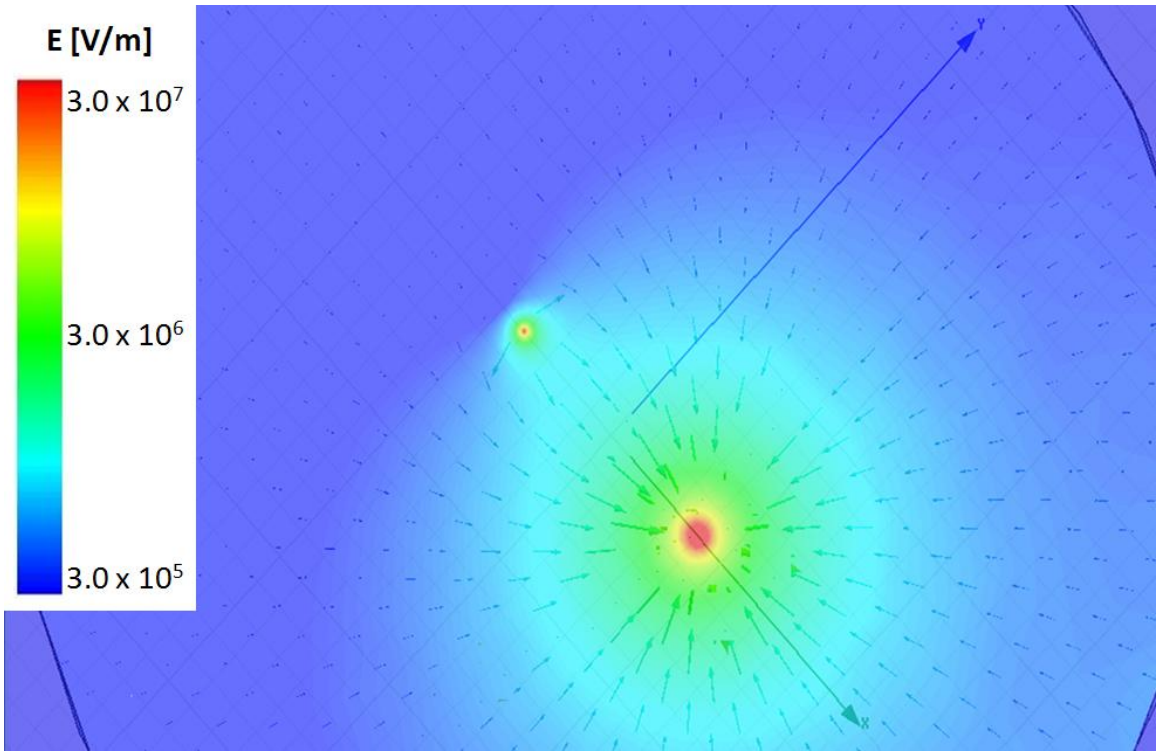

Figure 4.22: Simulation of electric field magnitude with the anode hard grounded.

In this model the electric field vectors are all pointing into the cathode from the anode and outside steel flange. The magnitude of the electric field near the cathode is much larger than the field near the anode, so the field enhancement factor is greatest in the

vicinity of the cathode. The ICCD imaging of streamers observed when the anode is hard grounded are shown below in Figure 4.23, gate time 10 ns:

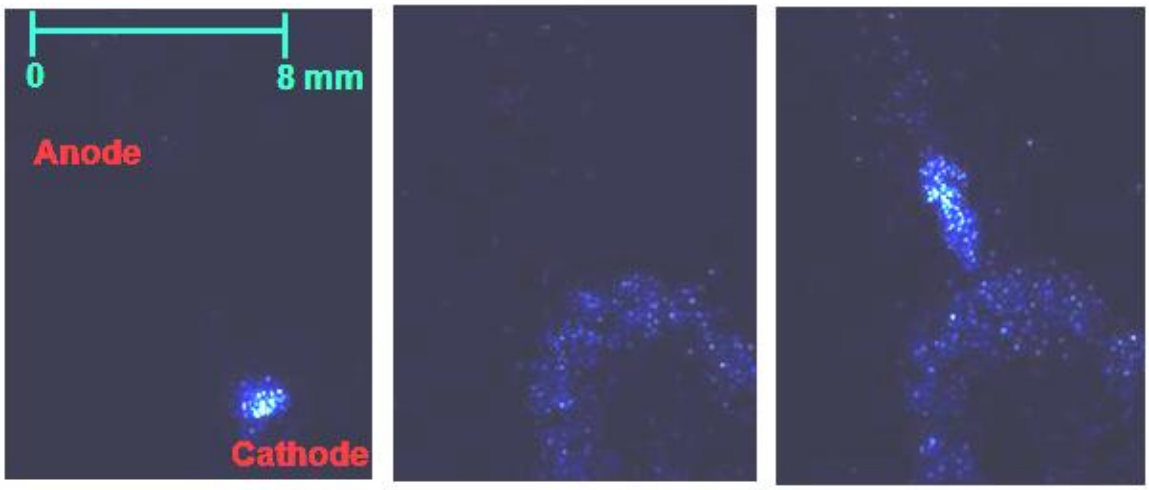

Figure 4.23: Streamer sequence observed when the anode is hard grounded, in air.

Note that in this configuration, the streamers observed are much different than in the previous two cases. The luminosity in the region surrounding the cathode is much larger than anywhere else at the beginning of the discharge, due to the large field enhancement factor. However once the initial electrons enter the space in the gap, they begin pushing away from each other in a region of low electric field magnitude. Limited photon activity is observed because the electron avalanches are not able to generate enough energy in this gap space. However eventually the local space charge becomes great enough to pull streamers from the anode and the connection occurs in the middle of the gap.

It is interesting that the three different cases of electric field geometry produce different streamer patterns. The primary difference is the location of high field regions, which determine the local field enhancement factor at the triple point. The simulated

electric field magnitude for each field geometry case is plotted below in Figure 4.24. While significant cathode directed streamers are observed for the symmetrical field case, the optimum geometry for streamer production is the hard grounded case. The electrons will be accelerated more into the anode (which is a point) in the hard grounded case, as compared to the negative high voltage case where they are simply pushed into the gap space and are diffused apart.

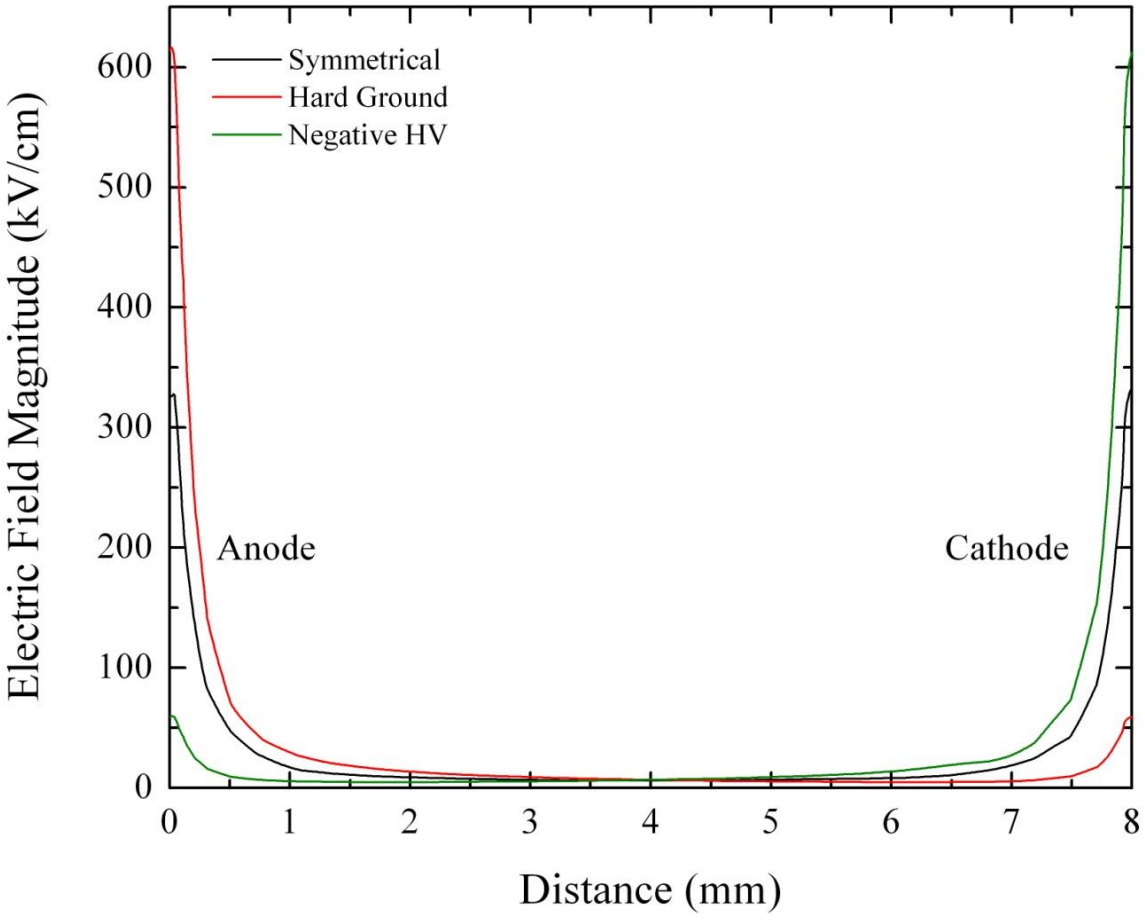

Figure 4.24: Electric field magnitude for each simulated field geometry case.

CHAPTER 5

CONCLUSIONS

The overall objective of this experiment was to observe VUV emission from pulsed atmospheric discharges, with emphasis on time resolved measurements which show the impact of VUV radiation on streamer propagation. A significant amount of VUV emission was observed from excited surface flashover events, and most of this activity was recorded during the nanoseconds leading into voltage collapse with limited VUV production for the remaining microseconds. The best fit of Boltzmann electronic temperature for the recorded emission profile in the flat region of limited absorption correction was 10 eV, which was calculated using a spectral simulation software package developed at Texas Tech. Virtually all emission lines between 120 and 180 nm observed from flashover correspond to excitations of atomic nitrogen and oxygen.

It was shown from corresponding electrical diagnostics that the VUV emission is tied to fluctuations of voltage from proposed streamer events which successfully bridge the flashover gap. Detailed streamer imaging from the atmospheric side agrees with the electrical and VUV emission diagnostics, in the sense that small current spikes coupled with voltage drops could be caused from VUV induced streamer activity. It is possible to simultaneously record VUV emission, electrical waveforms, and high resolution optical images with nanosecond timescales.

The results of the electrostatic field simulations support the observed streamer behavior for a number of field geometries. It was concluded from these simulations that

the field enhancement factor is maximized for the case when the cathode is hard grounded to the steel structure of the input window flange, and the resulting electric field at the triple point produces the most luminous cathode directed streamer activity in the study. Hard grounding of the anode produced a negative high voltage geometry, which produced slower and more diffuse anode directed streamers which agree with theory.

Because significant atomic excitations are observed from atmospheric discharges, it can be assumed that some mechanism exists which dissociates molecular gases during the breakdown process. Furthermore, the ionization energies for atmospheric gases are on the order of 12 - 15 eV, which correspond to wavelengths in the range of 70 – 90 nm [14]. A next generation VUV emission setup is currently in the planning stage which extends the sensitivity of the diagnostics into this range (see Figure 5.1).

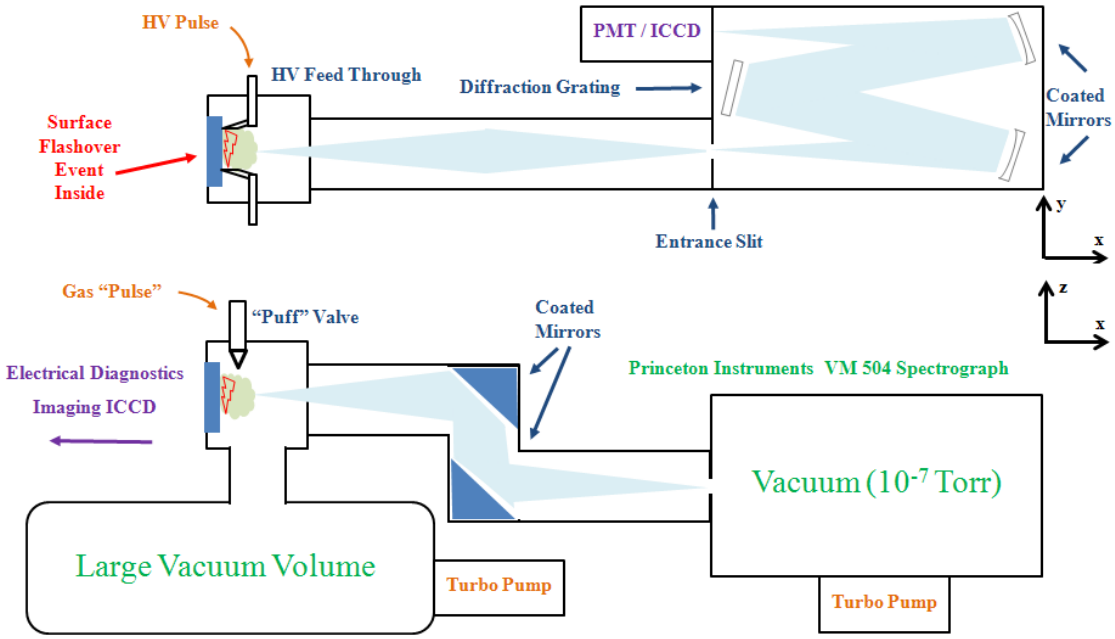

Figure 5.1: Next generation VUV experiment currently in the design phase.

Because the cutoff wavelength for MgF_2 is 115 nm, the idea is to create a discharge on the inside surface of the window dielectric so all light below this cutoff can still propagate through the beamline. In order to create an atmospheric discharge, a high density "puff" of gas is directed into the electrode gap at the moment the high voltage pulse is triggered. In addition, the MgF2 lens has been replaced with high reflectance mirrors, which should remove achromatic aberration from the imaged spectra. A large gas diffusion volume is attached in order to protect the turbo pumps during the gas insertion process. The proposed atomic emission spectrum (in addition to molecular N_2 and O_2 activity expected in the VUV, see Appendix C) which could be realized with this setup is given in Figure 5.2, for 10 eV Boltzmann temperature:

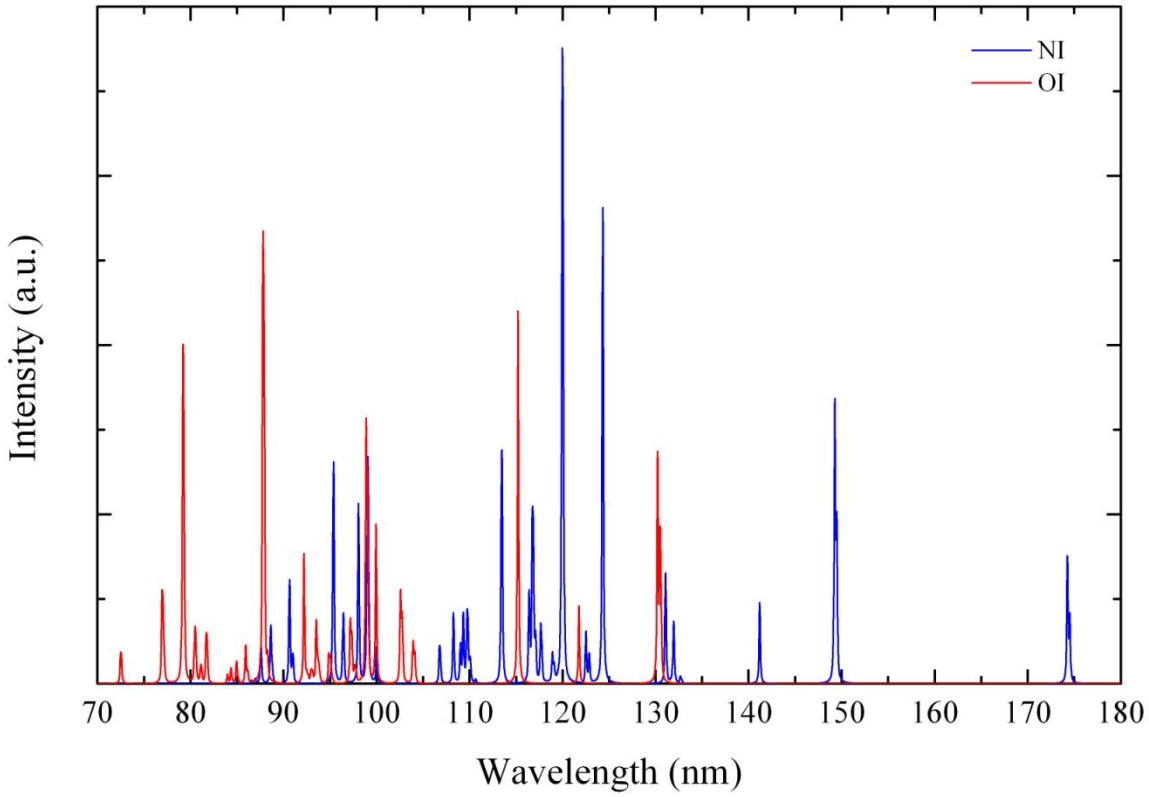

Figure 5.2: Extended simulation of VUV oxygen and nitrogen emission.

REFERENCES

[1] Y.P. Raizer, *Gas Discharge Physics*, Springer-Verlag, New York, (1997).

[2] E. Nasser, *Fundamentals of Gaseous Ionization and Plasma Electronics*, Wiley-Interscience, New York, (1971).

[3] J.M. Meek, J.D. Craggs, *Electrical Breakdown of Gases,* Oxford University Press, New York, (1953).

[4] E.M. van Veldhuizen, W.R. Rutgers, "Pulsed positive corona streamer propagation and branching," *J. Phys. D: Appl. Phys.*, Vol. 35, pp. 2169 – 2179, (2002).

[5] R. Ono, T. Oda, "Formation and structure of primary and secondary streamers in pulsed positive corona discharge – Effect of Oxygen and Applied Voltage," *J. Phys. D: Appl. Phys.*, Vol. 36, pp. 1952 – 1958, (2003).

[6] N.L. Aleksandrov, E.M Bazelyan, "Ionization processes in spark discharge plasmas," *Plasma Sources Sci. Technol.,* Vol. 8, pp. 285 – 294, (1999).

[7] G.V. Naidis, "On photoionization produced by discharges in air," *Plasma Sources Sci. Technol.*, Vol. 15, pp. 253 – 255, (2006).

[8] Y. Kashiwagi, H. Ito, K. Noguchi, K. Teranishi, S. Itoh, "Observation of VUV Emission Spectra from DC Positive Corona Discharge," *IEEJ Trans.*, Vol. 127 (9), pp. 537 - 542, (2007).

[9] T. Schramm, "Vacuum Ultraviolet Spectroscopy of DC Surface Flashover at Atmospheric Conditions," *P3E Internal Report, Texas Tech University,* (2008).

[10] Korth Kristalle GmbH, Material Datasheets, *www.korth.de,* (2010).

[11] A. Thorne, U. Litzen, S. Johansson, *Spectrophysics: Principles and Applications,* Springer, New York, (1999).

[12] G.F. Edmiston, "High Power Microwave Window Flashover at Atmospheric Pressures," *M.S.E.E. Degree Thesis, Texas Tech University*, (2005).

[13] P.A. Tipler, *Elementary Modern Physics*, W.H. Freeman, New York, (1992).

[14] M. Mitchner, C.H. Kruger, *Partially Ionized Gases*, Wiley-Interscience, New York, (1992).

[15] NIST Atomic Spectra Database, *www.nist.gov/physlab/data/asd.cfm*, (2010).

[16] D.J. Griffiths, *Introduction to Quantum Mechanics*, Prentice Hall, Upper Saddle River NJ, (2005).

[17] K. Morales, J. Krile, A. Neuber, H. Krompholz, "Dielectric Surface Flashover at Atmospheric Conditions with Unipolar Pulsed Voltage Excitation," *IEEE Trans. Dielectr. Electr. Insul.*, Vol. 14 (4), pp. 774 – 782, (2007).

[18] K. Morales, J. Krile, A. Neuber, H. Krompholz, "Pulsed Dielectric Surface Flashover in Nitrogen at Atmospheric Conditions," *IEEE Trans. Dielectr. Electr. Insul.*, Vol. 13 (4), pp. 803 – 809, (2006).

[19] J. Krile, A. Neuber, J. Dickens, H. Krompholz, "DC and Pulsed Dielectric Surface Flashover at Atmospheric Pressure," *IEEE Trans. Plasma Sci.*, Vol. 33 (4), pp. 1149 – 1154, (2005).

[20] G. Edmiston, J. Krile, A. Neuber, J. Dickens, H. Krompholz, "High Power Microwave Surface Flashover of a Gas-dielectric Interface at 90–760 torr," *IEEE Trans. Plasma Sci.*, Vol. 34 (5), pp. 1782 – 1788, (2006).

[21] J. Bedford, J.A. Swegle, E. Schamiloglu, *High Power Microwaves: Second Edition*, Taylor & Francis Group, New York, (2007).

[22] J. Krile, A. Neuber, H. Krompholz, "Effects of UV Illumination of Surface Flashover Under Pulsed Excitation," *IEEE Trans. Plasma Sci.*, Vol. 36 (2), pp. 332 – 340, (2008).

[23] J. Krile, G. Edmiston, K. Morales, A. Neuber, H. Krompholz, M. Kristiansen, "Similarities of dielectric surface flashover under atmospheric conditions for pulsed unipolar and RF excitation," *Laser Phys.,* Vol. 16 (1), pp. 194 – 201, (2006).

[24] G. Laity, A. Neuber, G. Rogers, K. Frank, "System for Time Resolved Spectral Studies of Pulsed Atmospheric Discharges in the Visible to VUV Range," *Review of Scientific Instruments,* (in review 2010).

[25] T.G. Rogers, A.A. Neuber, K. Frank, G. Laity, J.C. Dickens, "VUV Emission and Streamer Formation in Pulsed Dielectric Surface Flashover at Atmospheric Pressure," *IEEE Trans. Plasma Sci.,* (in review 2010).

[26] G. Rogers, A. Neuber, G. Laity, T. Schramm, J. Dickens, K. Frank, "VUV Emission from Dielectric Surface Flashover at Atmospheric Pressure," *Proc. 17th IEEE Int. Pulsed Power Conf.,* pp. 855 – 859, (2009).

[27] Solidtron / Silicon Power, Switch Model CCSTA14N40 Datasheet, *www.siliconpower.com*, (2009).

[28] List of Refraction Indices for Materials, *refractiveindex.info*, (2010).

[29] F.L. Pedrotti, L.S. Pedrotti, L.M. Pedrotti, *Introduction to Optics*, Prentice Hall, Englewood Cliffs NJ, (2007).

[30] Optical Ray Tracer v2.8, *www.arachnoid.com/OpticalRayTracer*, (2009).

[31] Princeton Instruments / Acton Research Corporation, VM-505 User's Manual, *www.princetoninstruments.com*, (2008).

[32] Pearson Electronics, Probe Model 2878 Datasheet, *www.pearsonelectronics.com*, (2009).

[33] Hamamatsu Corporation, PMT Model R8486 Datasheet, *www.hamamatsu.com*, (2009).

[34] Andor Technology, ICCD Model DH740 Datasheet, *www.andor.com*, (2009).

[35] Andor Technology, ICCD Model DH734 Datasheet, *www.andor.com*, (2005).

[36] Hamamatsu Corporation, Lamp Model L7293 Datasheet, *www.hamamatsu.com*, (2010).

[37] H. Bluhm, *Pulsed Power Systems: Principles and Applications*, Springer-Verlag, Berlin, (2006).

[38] U.S. Inan, A.S. Inan, *Engineering Electromagnetics*, Addison-Wesley, Menlo Park CA, (1999).

[39] A. Lofthus, P.H. Krupenie, "The Spectrum of Molecular Nitrogen,"*J. Phys. Chem. Ref. Data,* Vol. 6 (1), pp. 113 – 307, (1977).

[40] P.H. Krupenie, "The Spectrum of Molecular Oxygen,"*J. Phys. Chem. Ref. Data,* Vol. 1 (2), pp. 423 – 534, (1972).

APPENDIX A

PRINCIPLE OF ROGOWSKI COILS

A Rogowski coil is an extremely helpful measurement device used to record the instantaneous change of current in pulsed power experiments. These devices are discussed in detail in literature [37] and are briefly touched upon here. The basic topology of a Rogowski coil is shown below in Figure A.1:

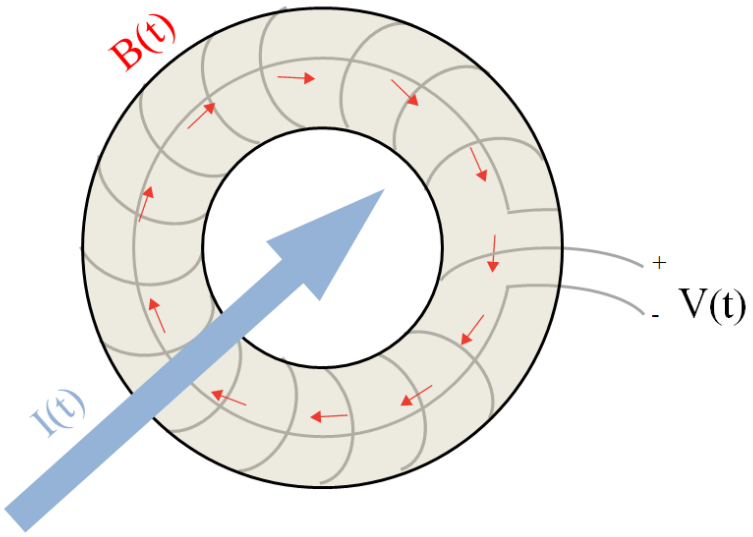

Figure A.1: Schematic of the basic electromagnetic field geometry for a Rogowski coil.

The fundamental concept is that a change in flowing current will cause an instantaneous change in magnetic flux through a closed surface some distance away from the current. This change in flux will induce an electromotive force in a coil wrapped around the closed surface, which can be recorded as a voltage. To begin, we note the magnetic field at some distance from a flowing current with the Biot - Savart Law [38]:

$$B(t) = \frac{\mu_0 I(t)}{2\pi r} \tag{A.1}$$

In a Rogowski coil, a wire is wrapped around a torus of material, which forms loops of cross sectional area *A* with loop spacing *s*. The induced signal (*V*) in the coil will be determined by the magnetic flux (Φ) generated in the cross sectional area of this coil:

$$V(t) = \frac{\partial \Phi}{\partial t} = \sum \vec{A} \cdot \dot{\vec{B}} = NA\dot{B}\cos(\theta) \tag{A.2}$$

where *N* is the number of turns in the Rogowski coil and ϑ is the angle the magnetic field vector makes with each loop (assumed $\vartheta \approx 0^o$ when current flows through the sensor). If the cross sectional area of each loop is the same, and the cross sectional area of each loop is small compared to the distance from the current source to the area (*r*), then the circumference at that distance is a function of the loop spacing and the number of total loops:

$$2\pi r \approx N s \tag{A.3}$$

Finally we can collect terms and find the signal voltage as a function of Rogowski coil parameters and current flowing through the sensor:

$$V(t) = NA\dot{B} = NA\frac{\mu_0}{2\pi r}\dot{I}(t) = \frac{A}{s}\mu_0 \dot{I}(t) \tag{A.4}$$

Therefore the sensor sensitivity is only a function of the loop area and spacing, and the current in the pulsed power circuit can be found by integrating the Rogowski signal.

APPENDIX B

ESTIMATION FOR THE NUMBER OF ATOMS IN DISCHARGE PLASMAS

```
# "Number of Atoms in Discharge Plasma Calculation"
# George Laity - 4/5/2010
# VUV Project (AFOSR)
# Center for Pulsed Power and Power Electronics
# Department of Electrical and Computer Engineering and Department of Physics
# Texas Tech University
restart :
Counts_A := 1085 : #ICCD Recorded for entire line @ 141.2 nm with 100 ns interval
t := 100·10^-9 : # ICCD gate time
QE := 0.132 : Gain := 30 : # Counts/Photoelectron @G = 125
Transmission_A := 0.37 : #MgF2@141.2nm
Reflectivity_A := 0.81 : #Mirror and Grating reflectance @ 141.2 nm
Lens := π·(34/2)^2 : #Lens cross section mm^2
SolidArea := 4·π·(4.75·25.4)^2 : #Total solid area @ lens distance from spark mm^2
Emission_A := Counts_A·(1/QE)·(1/Gain)·(1/Transmission_A)^3·(1/Reflectivity_A)^3·(SolidArea/Lens); #Number of photons emitted @ 141.2 nm in 100 ns
                                                    Emission_A := 2.050648027 10^6
T := 10 : Z := 450.71 : #Assumed temperature and partition function from NIST @ 10 eV
Wavenumber_A1 := 99663.912 : g_A1 := 4 : Einstein_A1 := 9.59·10^6 : # NIST data for the 141.1939 nm line
E_A1 := (1/Wavenumber_A1·10^7)^-1·1240; #Energy in eV of the parent energy level for the 141.1939 nm transition
                                                    E_A1 := 12.35832509
Population_A := Emission_A/(1 − exp(−Einstein_A1·t)); # Population of radiators for the 141.2 nm transition at t = 0
                                                    Population_A := 3.325065878 10^6
Percentage_A := g_A1·exp(−E_A1/T)/Z; # Percent of atoms which are at this energy level (12.36 eV)
                                                    Percentage_A := 0.002578977529
Atoms_A := Population_A/Percentage_A; # Number of nitrogen atoms in the system
                                                    Atoms_A := 1.289296181 10^9
Counts_B := 5088 : #ICCD Recorded for entire line @ 149 nm with 100 ns interval
Transmission_B := 0.441 : #MgF2@149 nm
Reflectivity_B := 0.79 : #Mirror and Grating reflectance @ 149 nm
Emission_B := Counts_B·(1/QE)·(1/Gain)·(1/Transmission_B)^3·(1/Reflectivity_B)^3·(SolidArea/Lens); #Number of photons emitted @ 149 nm in 100 ns
                                                    Emission_B := 6.121694824 10^6
Wavenumber_B1 := 86220.510 : g_B1 := 4 : Einstein_B1 := 3.13·10^8 : # NIST data for the 149.2625 nm line
Wavenumber_B2 := 86220.510 : g_B2 := 4 : Einstein_B2 := 3.51·10^7 : # NIST data for the 149.2820 nm line
Wavenumber_B3 := 86137.350 : g_B3 := 2 : Einstein_B3 := 3.72·10^8 : # NIST data for the 149.4675 nm line
E_B1 := (1/Wavenumber_B1·10^7)^-1·1240; #Energy in eV of the parent energy level for the 149.2625 nm transition
                                                    E_B1 := 10.69134324
E_B2 := (1/Wavenumber_B2·10^7)^-1·1240; #Energy in eV of the parent energy level for the 149.2820 nm transition
                                                    E_B2 := 10.69134324
E_B3 := (1/Wavenumber_B3·10^7)^-1·1240; #Energy in eV of the parent energy level for the 149.4675 nm transition
                                                    E_B3 := 10.68103140
Population_B := Emission_B·(1/(1 − exp(−Einstein_B1·t)) + 1/(1 − exp(−Einstein_B2·t)) + 1/(1 − exp(−Einstein_B3·t))); # Population of radiators for the 149 nm "area" transitions at t = 0
                                                    Population_B := 1.855374461 10^7
Percentage_B := 1/Z·(g_B1·exp(−E_B1/T) + g_B2·exp(−E_B2/T) + g_B3·exp(−E_B3/T)); # Percent of atoms which are at these energy levels
                                                    Percentage_B := 0.007618566685
Atoms_B := Population_B/Percentage_B; # Number of nitrogen atoms in the system
                                                    Atoms_B := 2.435332705 10^9
Error := 1 − (Atoms_B − Atoms_A)/Atoms_B;
                                                    Error := 0.5294127486
```

APPENDIX C

ENERGY LEVELS OF ATMOSPHERIC GASES

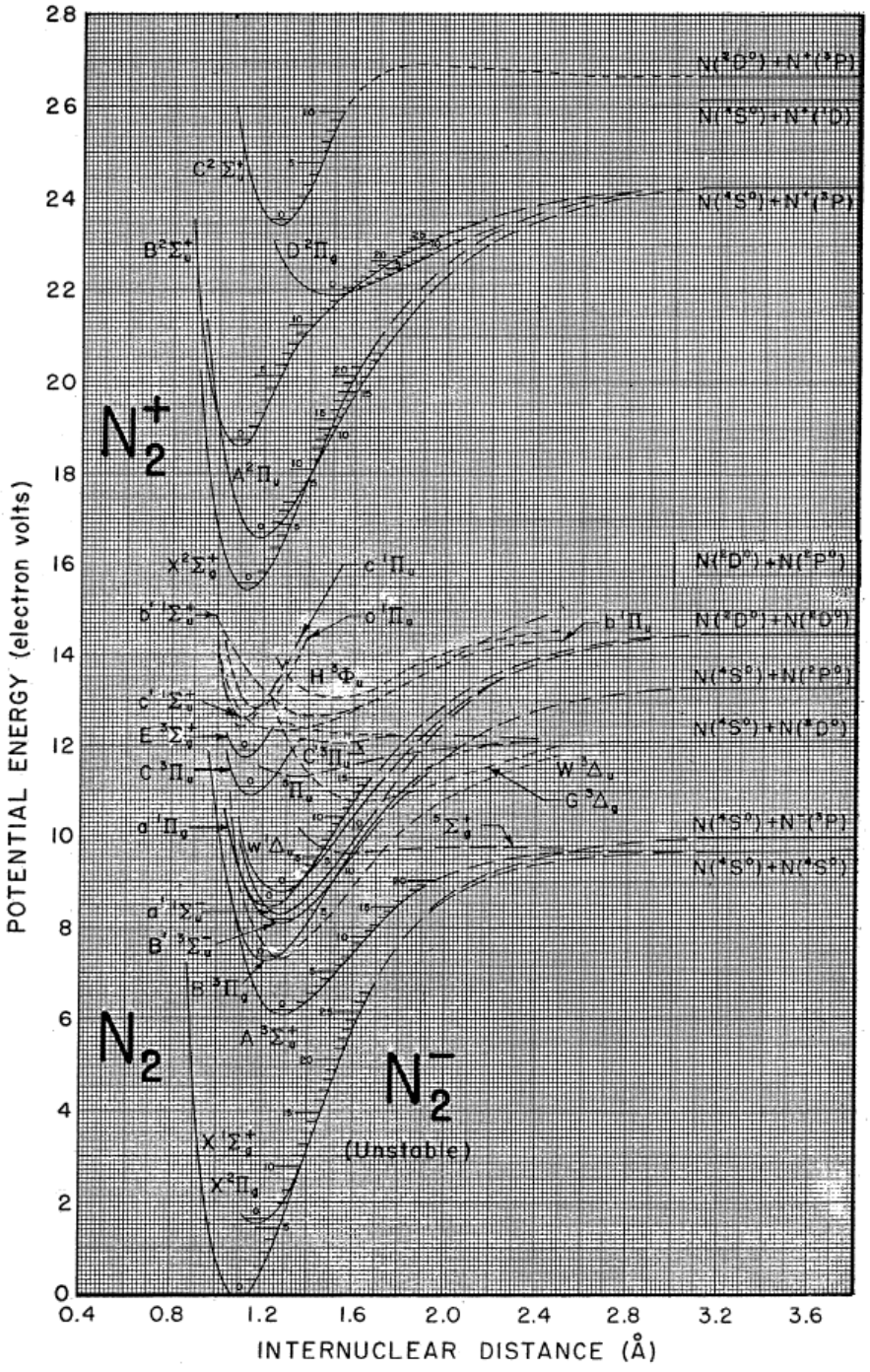

Figure C.1: Energy level diagram for molecular nitrogen [39].

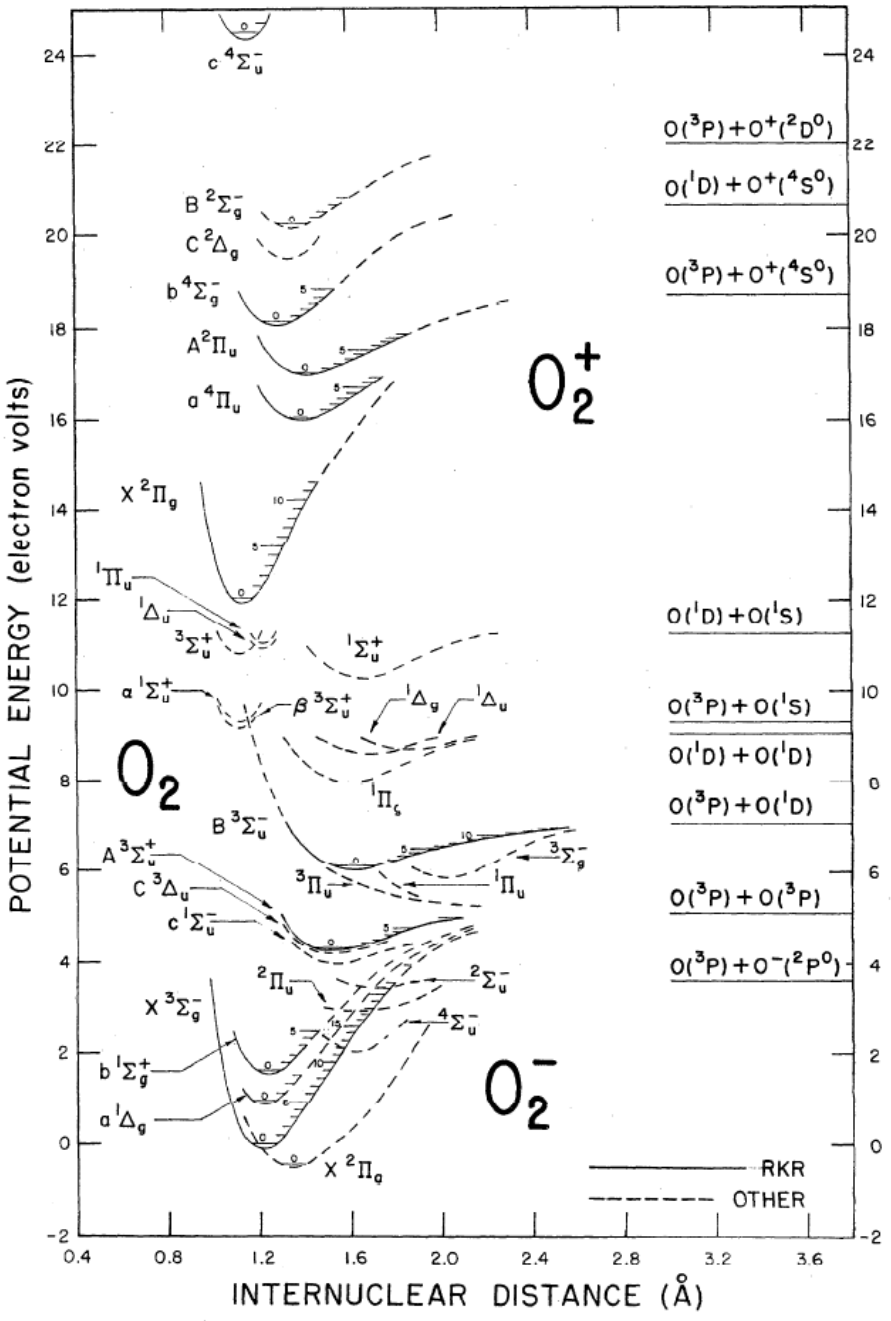

Figure C.2: Energy level diagram for molecular oxygen [40].